

# X-ray Reflectivity and Interfacial Tension Study of the Structure and Phase Behavior of the Interface between Water and Mixed Surfactant Solutions of $\text{CH}_3(\text{CH}_2)_{19}\text{OH}$ and $\text{CF}_3(\text{CF}_2)_7(\text{CH}_2)_2\text{OH}$ in Hexane

Sai Venkatesh Pingali,<sup>†</sup> Takanori Takiue,<sup>\*,‡</sup> Guangming Luo,<sup>†</sup> Aleksey M. Tikhonov,<sup>§</sup> Norihiro Ikeda,<sup>#</sup> Makoto Aratono,<sup>\*,‡</sup> and Mark L. Schlossman<sup>\*,†,||</sup>

Departments of Physics and Chemistry, University of Illinois at Chicago, 845 West Taylor Street, Chicago, Illinois 60607, Center for Advanced Radiation Sources, University of Chicago, and National Synchrotron Light Source, Beamline X19C, Brookhaven National Laboratory, Upton, New York 11973, Department of Chemistry, Faculty of Sciences, Kyushu University, Fukuoka 812-8581, Japan, and Department of Environment Science, Faculty of Human Environmental Science, Fukuoka Women's University, Fukuoka 813-8529, Japan

Received: September 11, 2004; In Final Form: November 5, 2004

The interface between water and mixed surfactant solutions of  $\text{CH}_3(\text{CH}_2)_{19}\text{OH}$  and  $\text{CF}_3(\text{CF}_2)_7(\text{CH}_2)_2\text{OH}$  in hexane was studied with interfacial tension and X-ray reflectivity measurements. Measurements of the tension as a function of temperature for a range of total bulk surfactant concentrations and for three different values of the molal ratio of fluorinated to total surfactant concentration (0.25, 0.28, and 0.5) determined that the interface can be in three different monolayer phases. The interfacial excess entropy determined for these phases suggests that two of the phases are condensed single surfactant monolayers of  $\text{CH}_3(\text{CH}_2)_{19}\text{OH}$  and  $\text{CF}_3(\text{CF}_2)_7(\text{CH}_2)_2\text{OH}$ . By studying four different compositions as a function of temperature, X-ray reflectivity was used to determine the structure of these monolayers in all three phases at the liquid–liquid interface. The X-ray reflectivity measurements were analyzed with a layer model to determine the electron density and thickness of the headgroup and tailgroup layers. The reflectivity demonstrates that phases 1 and 2 correspond to an interface fully covered by only one of the surfactants (liquid monolayer of  $\text{CH}_3(\text{CH}_2)_{19}\text{OH}$  in phase 1 and a solid condensed monolayer of  $\text{CF}_3(\text{CF}_2)_7(\text{CH}_2)_2\text{OH}$  in phase 2). This was determined by analysis of the electron density profile as well as by direct comparison to reflectivity studies of the liquid–liquid interface in systems containing only one of the surfactants (plus hexane and water). The liquid monolayer of  $\text{CH}_3(\text{CH}_2)_{19}\text{OH}$  undergoes a transition to the solid monolayer of  $\text{CF}_3(\text{CF}_2)_7(\text{CH}_2)_2\text{OH}$  with increasing temperature. Phase 3 and the transition regions between phases 1 and 2 consist of a mixed monolayer at the interface that contains domains of the two surfactants. In phase 3 the interface also contains gaseous regions that occupy progressively more of the interface as the temperature is increased. The reflectivity determined the coverage of the surfactant domains at the interface. A simple model is presented that predicts the basic features of the domain coverage as a function of temperature for the mixed surfactant system from the behavior of the single surfactant systems.

## Introduction

Solutions of two or more surfactants are widely used in industrial processes and have been studied scientifically for many years.<sup>1–4</sup> Use of multiple surfactants allows the physical and chemical properties of the solutions to be tuned for specific applications. Biological systems are believed to be actively adjusting the composition of, e.g., lipids in biomembranes to control life processes.

Studies of mixed surfactant solutions have focused on understanding the composition and structure of surfactant aggregates in the bulk solution as well as the influence of these surfactants on interfacial properties. In this paper, we limit our investigation to properties of the interface between water and a

hexane solution of mixed alkanol and fluoroalkanol (nonionic) surfactants. We present interfacial tension measurements as a function of temperature for different solution compositions and a structural study of the interface using X-ray reflectivity. X-ray reflectivity is one of the few techniques available for structural investigation of liquid–liquid interfaces.<sup>5</sup> Although neutron reflectivity has been used to study mixed surfactant monolayers at the liquid–vapor and solid–liquid interfaces, its utility for studies of the liquid–liquid interface has been limited.<sup>5,6</sup> Spectroscopic information is available from nonlinear optical probes of the liquid–liquid interface, but we are not aware of such studies of mixed monolayers at the liquid–liquid interface.<sup>7</sup> Because this is the first X-ray reflectivity study of a mixed surfactant system at the liquid–liquid interface, we are interested in exploring the utility and limitations of this technique as well as understanding the properties of the interface.

Studies of micelles in the bulk of mixed surfactant solutions indicate that the fluorocarbons and hydrocarbons often segregate, either by producing two different kinds of micelles, one of which is primarily fluorocarbon and the other primarily hydrocarbon,

\* Corresponding authors. E-mail: T.T., t.taksec@mbox.nc.kyushu-u.ac.jp; M.A., m.arascc@mbox.nc.kyushu-u.ac.jp; M.L.S., schloss@uic.edu.

<sup>†</sup> Department of Physics, University of Illinois at Chicago.

<sup>‡</sup> Kyushu University.

<sup>§</sup> University of Chicago and Brookhaven National Laboratory.

<sup>#</sup> Fukuoka Women's University.

<sup>||</sup> Department of Chemistry, University of Illinois at Chicago.

or by the separation of fluorocarbon and hydrocarbon regions within a single type of micelle.<sup>2,8–13</sup> This segregation has been attributed to the relatively weak interactions between the fluorocarbon and hydrocarbon species as compared to the stronger interaction of the fluorocarbon species with itself and the hydrocarbon species with itself. A similar segregation has been observed by atomic force microscopy in mixed Langmuir monolayers of fluorocarbon and hydrocarbon surfactants transferred onto a mica substrate.<sup>14,15</sup>

Earlier studies of the interfacial tension at 25.00 °C of mixtures of CH<sub>3</sub>(CH<sub>2</sub>)<sub>19</sub>OH and CF<sub>3</sub>(CF<sub>2</sub>)<sub>7</sub>(CH<sub>2</sub>)<sub>2</sub>OH at the water–hexane interface demonstrated the formation of three phases at the interface as either the surfactant composition or the bulk pressure was varied.<sup>16–19</sup> These studies indicated that two of the phases were essentially single surfactant condensed monolayers of either the alkanol or the fluoroalkanol whereas the third monolayer phase was an expanded state with alkanol and fluoroalkanol miscible in all proportions.

This manuscript extends these earlier studies of mixtures of CH<sub>3</sub>(CH<sub>2</sub>)<sub>19</sub>OH and CF<sub>3</sub>(CF<sub>2</sub>)<sub>7</sub>(CH<sub>2</sub>)<sub>2</sub>OH at the water–hexane interface to investigate the phase behavior as a function of temperature for a range of bulk composition. For selected compositions the interfacial tension measurements are supplemented by X-ray reflectivity measurements. The latter probes the interfacial electron density profile (electron density as a function of depth through the liquid–liquid interface) with subnanometer spatial resolution. Comparison of these profiles from the mixed system with profiles determined from single surfactant monolayers (either CH<sub>3</sub>(CH<sub>2</sub>)<sub>19</sub>OH or CF<sub>3</sub>(CF<sub>2</sub>)<sub>7</sub>(CH<sub>2</sub>)<sub>2</sub>OH) at the water–hexane interface<sup>20,21</sup> allows us to confirm the conclusions from the earlier tension studies that two of the monolayer phases are essentially single surfactant monolayers.<sup>16,17</sup> The X-ray reflectivity measurements indicate that the highest temperature phase, earlier referred to as the expanded phase, consists of domains of CF<sub>3</sub>(CF<sub>2</sub>)<sub>7</sub>(CH<sub>2</sub>)<sub>2</sub>OH separated by low-density gaseous monolayer regions of the interface or, in some cases, of both CF<sub>3</sub>(CF<sub>2</sub>)<sub>7</sub>(CH<sub>2</sub>)<sub>2</sub>OH and CH<sub>3</sub>(CH<sub>2</sub>)<sub>19</sub>OH domains separated by low-density gaseous monolayer regions of the interface. These new measurements are consistent with the earlier tension measurements and extend our understanding of the monolayer structure.

The X-ray reflectivity measurements also determine the coverage of the surfactant domains at the interface as a function of temperature. This is compared to the total interfacial density determined by the tension measurements. A simple model is presented that predicts the basic features of the domain coverage for the mixed surfactant system from the behavior of the single surfactant systems.

## Materials and Experimental Methods

**Materials.** 1-Eicosanol (CH<sub>3</sub>(CH<sub>2</sub>)<sub>19</sub>OH; denoted C<sub>20</sub>OH; purchased from Sigma Ltd.) and 1,1,2,2-tetrahydroheptadecafluorodecanol (CF<sub>3</sub>(CF<sub>2</sub>)<sub>7</sub>(CH<sub>2</sub>)<sub>2</sub>OH; denoted FC<sub>10</sub>OH; purchased from Lancaster Ltd.) were recrystallized seven and three times, respectively, from hexane. Their purity was checked by gas–liquid chromatography and interfacial tension measurements at the interface between water and a hexane solution. For the tension measurements, water was distilled three times from dilute alkaline permanganate solution and hexane once in the presence of metallic sodium particles. For the X-ray measurements, Barnstead NanoPure system water was used and *n*-hexane (99+%) purchased from Fluka was purified by passing six times through basic alumina in a chromatography column. Stability of the air–water surface tension and the hexane–water

interfacial tension were used to establish the purity of water and hexane, respectively.<sup>22,23</sup>

**Interfacial Tension.** The interfacial tension  $\gamma$  of the hexane solution of C<sub>20</sub>OH and FC<sub>10</sub>OH against water was measured as a function of temperature  $T$  and the total surfactant molality in hexane,  $m$ , at fixed composition of the mixture  $X_2 = m_2/m$  ( $m_2$  is the molality of FC<sub>10</sub>OH in hexane) under atmospheric pressure by the pendant drop method.<sup>24</sup> A glass cell with approximately 25 mL volume and syringe with a glass capillary were used for interfacial tension measurement. The drop of water, formed on the capillary tip, was photographed by a camera. The  $\gamma$  value was determined to within 0.05 mN/m by analyzing the shape of the drop.<sup>24</sup> Known densities of pure hexane and water were used to calculate the tension.<sup>25,26</sup>

Total interfacial density  $\Gamma^H$  vs temperature  $T$  was obtained from the interfacial tension measurements as follows. First, the  $\gamma$  values at a given  $T$  were plotted against total concentration  $m$ . Then the  $\Gamma^H$  values were calculated by applying the equation  $\Gamma^H = -(m/RT)(\partial\gamma/\partial m)_{T,p,x}$ . Interfacial density curves were also obtained from the X-ray reflectivity as described later.

Transition temperatures measured by interfacial tension and X-ray reflectivity differed by up to 2 °C (higher for the tension measurements). Because these two types of measurements were made in two different laboratories (tension in Japan, X-ray reflectivity in the U.S.) with different thermometers, the discrepancy in transition temperatures may be due to thermometer calibration. Alternatively, it may be due to slightly different sample concentrations or different levels of impurities in the samples. Tension measurements made in the U.S. (not published in this paper) with the same sample cell used for the X-ray reflectivity had transition temperatures that agreed with those determined by X-ray reflectivity. Also, values of interfacial excess entropy determined by tension measurements in the two laboratories agreed.

**Sample Cell.** Samples for X-ray measurements were contained in a stainless steel sample cell described elsewhere.<sup>27</sup> The cell was cleaned with soap and water, methanol, acetone, rinsed with water, and then allowed to sit in hexane at 50 °C for several hours. Mylar sheets were used as X-ray windows and wall inserts such that the liquid–liquid interface was in contact only with Mylar. After partially filling the sample cell with 100 mL of water and waiting 30 min, the water surface was aspirated by a glass pipet. The hexane solution of surfactants was then poured on top of the water. The interfacial area was 76 mm × 100 mm (along the beam by transverse). The sample cell was placed in a two-stage cylindrical aluminum thermostat and temperature controlled to  $\pm 0.005$  °C.<sup>27</sup> Two thermistors mounted within the stainless steel sample cell immediately above and below the liquid chamber measured the sample temperature and allowed us to determine when the sample cell had thermally equilibrated. A pressure release valve in the gas phase above the bulk liquids is open during temperature changes so the bulk pressure is at atmospheric pressure.

**X-ray Reflectivity.** X-ray reflectivity was measured at beamline X19C at the National Synchrotron Light Source (Brookhaven National Laboratory) with a liquid surface instrument and measurement techniques described in detail elsewhere.<sup>21,27–29</sup> The kinematics of specular reflectivity is illustrated in Figure 1a. The reflectivity data are measured as a function of the wave vector transfer normal to the interface,  $Q_z = (4\pi/\lambda) \sin \alpha$  (the in-plane wave vector components  $Q_x = Q_y = 0$  where  $\lambda = 0.825 \pm 0.002$  Å is the X-ray wavelength and  $\alpha$  is the angle of reflection). Therefore, specular reflection probes

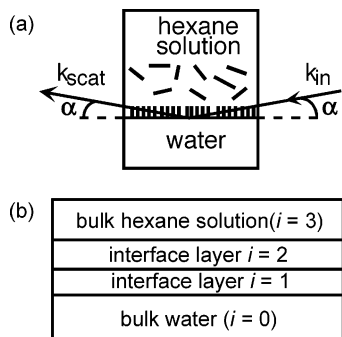


**Figure 1.** (a) X-ray kinematics for reflectivity from the interface between water and a hexane solution of surfactants. (b) Layer model for a monolayer of surfactants at the water–hexane interface. Domains of FC<sub>10</sub>OH are modeled with one layer, domains of C<sub>20</sub>OH are modeled with two layers (for the headgroup and tailgroup regions).

structure normal to the interface, but averaged over the in-plane region of the X-ray footprint on the interface.

The X-rays penetrate through the upper bulk hexane solution then reflect off the water–hexane interface. Absorption lengths for hexane and water at our X-ray wavelength are 19.2 and 5.6 mm, respectively. The reflectivity data consist of measurements of the X-ray intensity reflected from the sample interface normalized to the incident intensity measured just before the X-rays strike the interface. The reflectivity data are further modified by subtracting a background measured as previously described.<sup>27</sup> To set the incident beam size and vertical divergence (to 20  $\mu$ rad), two slits placed approximately 60 cm apart were used immediately prior to the liquid sample. The slit gaps were typically 5–10  $\mu$ m in the vertical at the smallest reflection angles (horizontal slit gaps were 10 mm, much larger than the horizontal beam size of  $\sim$ 2 mm). The sample was followed by a slit with a vertical gap of  $\sim$ 2 mm to reduce the background scattering, and a scintillator detector was preceded by a slit with a vertical gap of 0.8 or 1.2 mm that sets the detector resolution. The vertical angular acceptance  $\Delta\beta$  of the detector was set to be either  $1.18 \times 10^{-3}$  or  $1.78 \times 10^{-3}$  rad.

Tests for radiation damage were made throughout the X-ray measurements by repeating measurements on the same sample. No radiation damage was evident.

X-ray reflectivity  $R(Q_z)$  from the water–hexane interface can be interpreted to yield the electron density profile by the use of the first Born approximation, written as<sup>30</sup>

$$\frac{R(Q_z)}{R_F(Q_z)} \approx \left| \frac{1}{(\rho_W - \rho_H)} \int dz \frac{d\langle\rho_e(z)\rangle_{xy}}{dz} \exp(iQ_z z) \right|^2 \quad (1)$$

where  $z$  is in the normal direction,  $\langle\rho_e(z)\rangle_{xy}$  is the electron density profile averaged over the surface area of the interface (in the  $x$ – $y$  plane),  $\rho_W$  and  $\rho_H$  are the electron densities of bulk water and hexane, respectively (e.g.,  $\rho_H = 0.230 \text{ e}^-/\text{\AA}^3$  and  $\rho_W = 0.3337 \text{ e}^-/\text{\AA}^3$  at  $T = 20 \text{ }^\circ\text{C}$ ), and the Fresnel reflectivity ( $R_F$ ) from an ideally smooth interface is expressed as<sup>31,32</sup>

$$R_F(Q_z) \approx \left| \frac{Q_z - Q_z^T}{Q_z + Q_z^T} \right|^2 \quad (2)$$

where  $Q_z^T = (Q_z^2 - Q_c^2)^{1/2}$  is the  $z$ -component of the wave vector transfer with respect to the lower phase. Total reflection of X-rays from the lower phase occurs for  $Q_z \leq Q_c$  where the critical wave vector transfer is  $Q_c = 4(\pi r_e (\rho_W - \rho_H))^{1/2} \approx 0.012 \text{ \AA}^{-1}$  ( $r_e$  is the classical electron radius).

Monolayers of surfactants at the water–hexane interface are modeled by layers illustrated in Figure 1b and described by eq 3. As shown previously, one layer is adequate to model a monolayer of FC<sub>10</sub>OH, two layers are required to model the headgroup and tailgroup regions of a monolayer of C<sub>20</sub>OH.<sup>20,21</sup> Interfaces at the top and bottom of each layer will fluctuate with capillary waves.<sup>33,34</sup> These waves produce a broadening of the time-averaged interface probed by the X-rays. Capillary wave theory predicts that the interface is broadened with an error function of interfacial width or roughness,  $\sigma$ . The electron density for the two layer interface, illustrated in Figure 1b, is given by

$$\frac{\langle\rho_e(z)\rangle_{xy}}{\rho_W} = \frac{\rho_H}{\rho_W} + \frac{1}{2} \sum_{i=0}^2 \left[ (\rho_i - \rho_{i+1}) \left\{ 1 + \text{erf} \left( \frac{z + \sum_{j=0}^i z_j}{\sigma\sqrt{2}} \right) \right\} \right]$$

with

$$\text{erf}(z) = \frac{2}{\sqrt{\pi}} \int_0^z dt e^{-t^2} \quad (3)$$

Note that electron densities quoted in this paper are normalized to the bulk density of water such that  $\rho_0 = \rho_W/\rho_W \equiv 1.0$  (bulk water),  $\rho_3 = \rho_H/\rho_W = 0.68$  (bulk hexane at  $T = 20 \text{ }^\circ\text{C}$ ), and  $\rho_i$  is the normalized electron density of layer  $i$ .

Studies of the water–hexane interface containing either FC<sub>10</sub>OH or C<sub>20</sub>OH show that at higher temperatures the surfactants desorb from the interface, leaving regions with a very low density of surfactants. We have found that these gaseous monolayers can be modeled by the reflectivity from a simple interface,<sup>20,21</sup> given by

$$R(Q_z) \approx \left| \frac{Q_z - Q_z^T}{Q_z + Q_z^T} \right|^2 \exp(-Q_z Q_z^T \sigma^2) \quad (4)$$

Earlier measurements have shown that the interfacial width  $\sigma$  for gaseous monolayers of C<sub>20</sub>OH is approximately 5.5  $\text{\AA}$ , larger than the value calculated from capillary waves (typically about 3.5  $\text{\AA}$  at  $T = 45 \text{ }^\circ\text{C}$ ).<sup>21,35</sup> The reflectivity for the gaseous monolayer can be analyzed by adding an additional interfacial width, the intrinsic width, that models structure due to the small number of surfactants at the interface.<sup>36,37</sup> This intrinsic width does not provide information about the molecular conformation in the gaseous phase, but only allows us to model the reflectivity in this region in the simplest possible manner. For gaseous monolayers the width is given by a combination of an intrinsic profile width  $\sigma_o$  and a resolution dependent capillary wave contribution,<sup>21,36,38–40</sup>

$$\sigma_{\text{gas}}^2 = \sigma_o^2 + \sigma_{\text{cap}}^2 \equiv \sigma_o^2 + \frac{k_B T}{2\pi\gamma} \int_{q_{\text{min}}}^{q_{\text{max}}} dq \frac{q}{q^2 + \xi_{\parallel}^{-2}} \approx \sigma_o^2 + \frac{k_B T}{2\pi\gamma} \ln \left( \frac{q_{\text{max}}}{q_{\text{min}}} \right) \quad (5)$$

where  $\sigma_o$  is the intrinsic width,  $k_B T$  is Boltzmann's constant times temperature,  $\gamma$  is the interfacial tension, the correlation length,  $\xi_{\parallel}$ , is given by  $\xi_{\parallel}^2 = \gamma/\Delta\rho_m g$ ,  $\Delta\rho_m$  is the mass density difference of the two bulk phases, and  $g$  is the gravitational acceleration. The wave vector  $q$  represents the in-plane wave vector of the capillary waves. The approximation in eq 5 is calculated by choosing  $q_{\text{max}}$  (the cutoff for the smallest wavelength capillary waves that the interface can support), and using  $q_{\text{min}} = (2\pi/\lambda)\Delta\beta \sin \alpha$  determined by the incident angle  $\alpha$  and the angular acceptance of the detector  $\Delta\beta$ .<sup>23,39,40</sup> The

correlation length  $\xi_{||}$  can be neglected because  $q_{\min} \gg \xi_{||}^{-1}$ . We have chosen  $q_{\max} = 2\pi/5 \text{ \AA}^{-1}$ , where  $5 \text{ \AA}$  is a typical nearest neighbor distance of closest approach for alkanes, though there is little theoretical guidance for the correct choice of  $q_{\max}$ . For both eqs 3 and 5, an intrinsic profile fluctuates with capillary waves. For eq 3 the intrinsic profile is given by the layers in Figure 1b, for eq 5 we chose a simple interfacial width  $\sigma_0$  for the profile.

For many temperatures and concentrations the interface is not a homogeneous surfactant monolayer but consists of domains of surfactants. If the spatial coherence length of the X-rays in the plane of the interface is much larger than the domains, then the X-rays reflected from neighboring domains interfere nearly coherently. If the domains are much larger than the coherence length, then the interference between neighboring domains is nearly incoherent. If incoherent, then the intensity of the reflected electromagnetic fields should add; if coherent, the amplitudes of the reflected electromagnetic fields will add.<sup>41,42</sup> An example of incoherent reflectivity for an interface with two distinct types of domains is given by

$$R_{\text{inc}}(Q_z) = CR_1(Q_z) + (1 - C)R_2(Q_z) \quad (6)$$

where  $R_1$  and  $R_2$  refer to the X-ray reflectivity from a pure monolayer of molecules from domains 1 and 2, respectively (see eq 1). The domain coverage  $C$  is the fraction of interface occupied by that type of domain, coverage of the other domain is given by  $1 - C$ . A similar example for coherent reflectivity is provided by

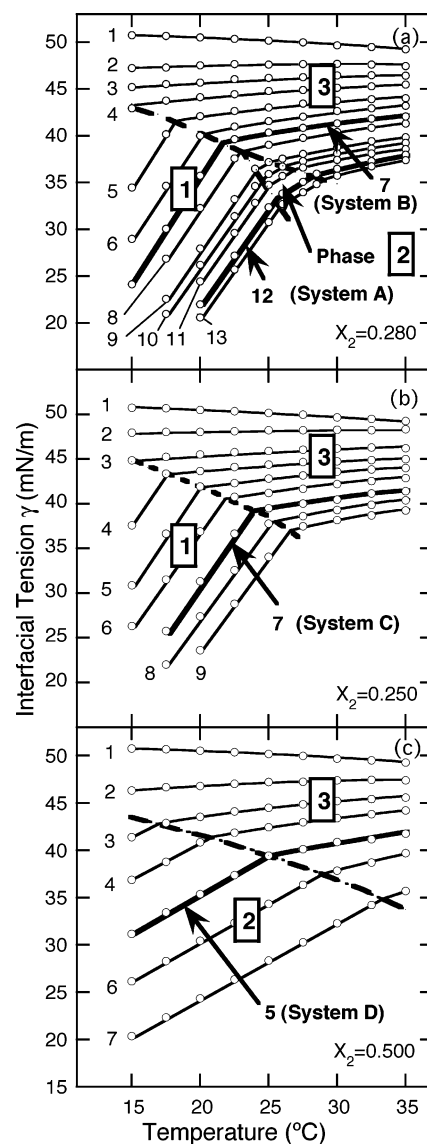
$$R_{\text{coh}}(Q_z) = |Cr_1(Q_z) + (1 - C)r_2(Q_z)|^2 \quad (7)$$

where  $r_1$  and  $r_2$  are the reflection amplitudes of the two domains at the interface. For a two-domain interface, the two fitting parameters are the interfacial width  $\sigma$  and the domain coverage  $C$  of one type of domain. The extension to interfaces with three types of domains is straightforward with the addition that two different coverages for two of the three types of domains are required as fitting parameters. The one caveat to this fitting procedure is that, independent of temperature, gaseous domains are treated as a pure water-hexane interface, with a total interfacial width of  $5.5 \text{ \AA}$  as we measured for a homogeneous gaseous phase in single surfactant systems.

## Data and Analysis

**Interfacial Tension.** Phase diagrams of the mixed surfactant system ( $C_{20}OH$  and  $FC_{10}OH$ ) at the water-hexane interface for three different values of  $X_2$  (ratio of  $FC_{10}OH$  concentration to total surfactant concentration) are shown in Figure 2. The phase diagram for  $X_2 = 0.28$  indicates the presence of three phases and a triple point, whereas the diagrams for  $X_2 = 0.25$  and  $X_2 = 0.5$  indicate the presence of one phase transition separating two phases.

For our X-ray studies we chose four different paths through these phase diagrams, labeled systems A–D in Figure 2, that allowed us to study all the phases. Choice of the overall concentration  $m$  and the  $FC_{10}OH$  molar fraction  $X_2$  determined the four paths and are specified in Table 1. The slope of the solid lines in these plots yields the interfacial excess entropy per unit area  $S_a^\sigma = -(d\gamma/dT)_{p,X_2,m}$ . The entropies for the different phases of systems A–D are listed in Table 1. Typical values are  $-2.2 \text{ mJ}/(\text{m}^2 \text{ K})$  in phase 1,  $-0.8 \text{ mJ}/(\text{m}^2 \text{ K})$  in phase 2, and  $-0.2 \text{ mJ}/(\text{m}^2 \text{ K})$  in phase 3.



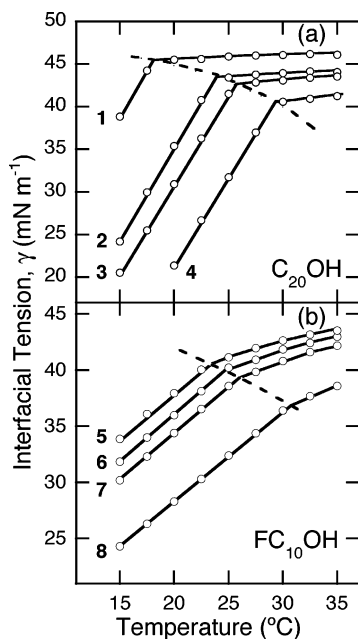
**Figure 2.** Interfacial tension vs temperature for three different values of the molal ratio of fluorinated to total surfactant concentration  $X_2 =$  (a) 0.28, (b) 0.25, and (c) 0.50. Solid lines are a guide for the eye at constant total surfactant molality  $m$  (mmol/kg). Bold solid lines labeled system A, B, C, or D indicate the four concentrations studied with X-ray reflectivity. Bold dashed lines indicate phase boundaries between phases labeled by boxed numbers 1, 2, or 3. (a)  $m$  given by (1) 0, (2) 1.991, (3) 3.496, (4) 4.978, (5) 7.488, (6) 9.958, (7) 12.46 (system B), (8) 14.94, (9) 18.21, (10) 19.99, (11) 22.00, (12) 25.06 (system A), (13) 27.00. (b)  $m$  given by (1) 0, (2) 1.980, (3) 3.989, (4) 5.990, (5) 8.511, (6) 11.21, (7) 15.00 (system C), (8) 18.00, (9) 22.50. (c)  $m$  given by (1) 0, (2) 1.982, (3) 4.018, (4) 5.740, (5) 8.802 (system D), (6) 12.50, (21) 20.00.

Figure 3 shows tension curves for single surfactant systems consisting of either  $C_{20}OH$  or  $FC_{10}OH$  at the water-hexane interface. To facilitate a comparison between the behavior of the single surfactant systems and the mixed surfactant systems, the concentrations for these systems nearly match the values of the concentrations for the surfactants used in the mixed systems A–D. Typical values of  $S_a^\sigma$  are  $-2.1 \text{ mJ}/(\text{m}^2 \text{ K})$  for the  $C_{20}OH$  single surfactant system in its lower temperature phase,  $-0.82 \text{ mJ}/(\text{m}^2 \text{ K})$  for the  $FC_{10}OH$  single surfactant system in its lower temperature phase, and  $-0.1$  or  $-0.2 \text{ mJ}/(\text{m}^2 \text{ K})$  in the high-temperature phase of  $C_{20}OH$  or  $FC_{10}OH$ , respectively (Table 2). These values correspond closely to the values in phases 1–3 of the mixed systems (Table 1), leading to the expectation that

**TABLE 1: Systems Studied by X-rays<sup>a</sup>**

systems label	$m$ ( $\pm 0.025$ ) (mmol/kg)	$X_2$ ( $\pm 0.001$ )	temp range ( $^{\circ}\text{C}$ )	$T^*$ ( $^{\circ}\text{C}$ )		$S_a^{\sigma}$ [ $\pm 0.05$ mJ/(m <sup>2</sup> K)]		
				I	II	1	2	3
A	25.06	0.280	21.0–57.5	25.50	28.20	-2.04	-0.84	-0.37
B	12.46	0.280	16.0–55.9	21.60	N/A	-2.32	N/A	-0.19
C	15.00	0.250	18.0–57.5	23.70	N/A	-2.18	N/A	-0.20
D	8.80	0.500	19.0–55.4	25.00	N/A	N/A	-0.82	-0.21

<sup>a</sup> The total bulk surfactant concentration is  $m$  ( $=m_H + m_F$ );  $X_2$  ( $=m_F/m$ ) is the ratio of the fluorinated bulk surfactant concentration to the total bulk surfactant concentration;  $T^*$  is the transition temperature (I and II refer to two transitions);  $S_a^{\sigma}$  is the interfacial excess entropy per unit area and 1–3 are the three phases as in Figure 2.



**Figure 3.** Interfacial tension variation with temperature for single surfactant systems at the water–hexane interface. The illustrated concentrations correspond to the concentration of that surfactant in the mixed systems A–D as indicated in parentheses. (a) C<sub>20</sub>OH at concentrations (mmol/kg): (1) 4.40 (D); (2) 8.97 (B); (3) 11.25 (C); (4) 18.04 (A). (b) FC<sub>10</sub>OH at concentrations (mmol/kg): (5) 3.485 (B); (6) 3.986 (C); (7) 4.502 (D); (8) 6.982 (A).

phase I is similar to the lower temperature phase in a C<sub>20</sub>OH single surfactant system, phase II is similar to the lower temperature phase in a FC<sub>10</sub>OH single surfactant system, and phase III is similar to the higher temperature phases of the single surfactant systems. As will be shown, these expectations are consistent with the X-ray measurements that assign phase I to be a monolayer of C<sub>20</sub>OH, phase II to be a monolayer of FC<sub>10</sub>OH, and phase III to consist of domains of either one or both of the surfactants along with gaseous regions between the surfactant domains.

**X-ray Reflectivity. Single Surfactant Monolayers.** Analysis of single surfactant systems of C<sub>20</sub>OH and FC<sub>10</sub>OH at the water–hexane interface has been previously discussed.<sup>20,21</sup> Here, we present a more complete X-ray data set for C<sub>20</sub>OH than previously published<sup>21</sup> and provide an overview of both single surfactant systems for purposes of comparison with the mixed surfactant system. We show that below the phase transition the interfaces for both the C<sub>20</sub>OH and FC<sub>10</sub>OH systems are nearly fully covered by the surfactant. The FC<sub>10</sub>OH monolayer is a close-packed solid, and the C<sub>20</sub>OH monolayer has liquid ordering. Above the transition the interface with C<sub>20</sub>OH consists of a small number of surfactants, but the interface with FC<sub>10</sub>OH has many domains separated by regions of gaseous monolayer.

(a) C<sub>20</sub>OH. Figure 4 illustrates X-ray reflectivity curves from an interface between water and a 15 mmol/kg solution of C<sub>20</sub>OH in hexane. The interfacial roughness, the headgroup and tailgroup layer thicknesses, and the electron density parameters from a two-layer fit (eq 3) to the data measured at  $T = 19.38$   $^{\circ}\text{C}$  are listed in Table 3. The fit value for the roughness agrees with the value calculated from the expression for  $\sigma_{\text{cap}}$  in eq 5. The value of 0.80 for the tailgroup electron density agrees with the density of 0.81 determined for the alkyl chains of bulk liquid alkanes and alkanols just above their freezing point. This indicates a liquid ordering of the C<sub>20</sub>OH chains in the monolayer at the water–hexane interface. As discussed elsewhere, the small headgroup ( $-\text{CH}_2\text{OH}$ ) produces large uncertainties in the layer thickness and electron density.<sup>21</sup> A better parametrization is in terms of the maximum electron density  $\rho_{\text{max}}$  in the headgroup region (Table 3).

The reflectivity data at the highest temperature can be fit by the model of a simple interface described by eqs 4 and 5. The reflectivity data at intermediate temperatures (excluding the lowest and highest temperature) are fit using eqs 6 and 7 that describe the monolayer in terms of domains. The values  $R_1$  and  $R_2$  (or  $r_1$  and  $r_2$ ) are chosen to be the X-ray reflectivities (or amplitudes) determined from the fits to the lowest temperature data and the highest temperature data, respectively. The domain coverage (the fraction of the interface covered by domains of the condensed phase) and roughness are the only fitting parameters used to fit the intermediate temperature data. However, the fit values of the interfacial roughness are within error bars of the values calculated by capillary wave theory using eq 5. This calculation used our measured values of the interfacial tension for that temperature and an intrinsic profile width  $\sigma_0 = 0$  for the condensed phase and  $\sigma_0 = 3.5$   $\text{\AA}$  for the gas phase (as determined by our lowest and highest temperature measurements, respectively).

Figure 4b illustrates values for domain coverage  $C$  determined from fitting the data in Figure 4a. For these data, the domain coverage is essentially independent of the choice of coherent or incoherent reflectivity given by eqs 6 and 7. Figure 4b indicates that the interface is fully covered by the monolayer below the transition temperature. Above the transition the coverage is approximately 0.07. This indicates that 7% of the interface is covered by domains that have the same structure as the condensed monolayer phase present below the transition. However, it is difficult for our measurements to distinguish between a phase with coverage this close to zero and a homogeneous monolayer. So, an alternative explanation consistent with the error bars on our data is that the interface above the transition contains a low density of C<sub>20</sub>OH molecules that are not aggregated into domains.

(b) FC<sub>10</sub>OH. Figure 5a illustrates X-ray reflectivity curves from an interface between water and a 5.0 mmol/kg solution of FC<sub>10</sub>OH in hexane. As discussed elsewhere, these data are not sensitive to the presence of the headgroup and are well fit by a

TABLE 2: Single Surfactant Systems<sup>a</sup>

corresponding mixed system	$m_F (\pm 0.025)$ (mmol/kg)	$T^*_{\text{F}} (\text{°C})$	$m_H (\pm 0.025)$ (mmol/kg)	$T^*_{\text{H}} (\text{°C})$	$S^{\sigma}_{a,H} [\pm 0.05 \text{ mJ/m}^2 \text{ K}]$		$S^{\sigma}_{a,F} [\pm 0.05 \text{ mJ/m}^2 \text{ K}]$	
					$T < T^*_{\text{H}}$	$T > T^*_{\text{H}}$	$T < T^*_{\text{F}}$	$T > T^*_{\text{F}}$
A	6.982	31.0	18.04	29.0	-2.07	-0.14	-0.81	-0.04
B	3.485	23.0	8.97	24.0	-2.19	-0.06	-0.80	-0.22
C	3.986	25.0	11.25	25.5	-2.12	-0.10	-0.84	-0.27
D	4.502	26.0	4.40	18.0	-2.16	-0.04	-0.84	-0.29

<sup>a</sup> Properties of single surfactant systems that have very similar concentrations for the individual surfactants as in the mixed systems described in Table 1. Each row lists properties for two separate single surfactant systems (a FC<sub>10</sub>OH and a C<sub>20</sub>OH system). Concentrations  $m_H$  and  $m_F$  are respectively the bulk C<sub>20</sub>OH and FC<sub>10</sub>OH surfactant concentrations;  $T^*_{\text{H}}$  and  $T^*_{\text{F}}$  are the phase-transition temperatures for C<sub>20</sub>OH and FC<sub>10</sub>OH single surfactant systems;  $S^{\sigma}_{a,H}$  and  $S^{\sigma}_{a,F}$  are the interfacial excess entropy per unit area for C<sub>20</sub>OH and FC<sub>10</sub>OH single surfactant systems (below and above the transition).

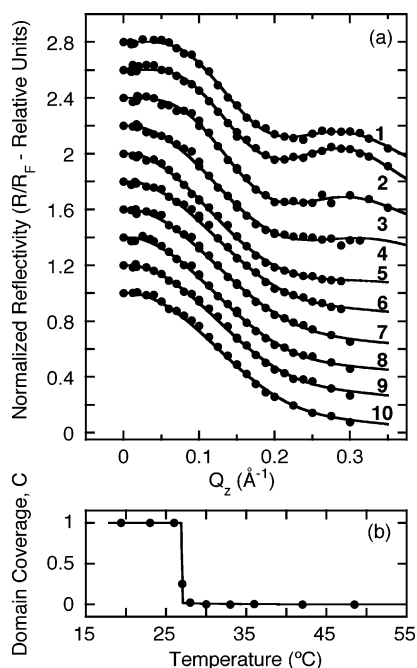


**Figure 4.** (a) X-ray reflectivity normalized to the Fresnel reflectivity from the interface between water and a 15 mmol/kg solution of C<sub>20</sub>OH in hexane: (1)  $19.38 \pm 0.02$  °C, (2)  $23.02 \pm 0.04$  °C, (3)  $25.93 \pm 0.03$  °C, (4)  $26.91 \pm 0.03$  °C, (5)  $27.91 \pm 0.03$  °C, (6)  $29.95 \pm 0.04$  °C, (7)  $32.90 \pm 0.06$  °C, (8)  $35.90 \pm 0.05$  °C, (9)  $41.88 \pm 0.03$  °C, (10)  $48.48 \pm 0.02$  °C. Data for different temperatures are progressively offset by 0.2 ( $R/R_F = 1$  at  $Q_z = 0$ ). Solid lines are fits described in the text. (b) Domain coverage as a function of temperature determined by the data in part a.<sup>21</sup> The solid line is a fit described elsewhere.<sup>21</sup>

single layer (Table 2).<sup>20</sup> At  $T = 18$  °C the layer thickness corresponds to the all-trans length of the fluorinated part of the tailgroup, the electron density is in agreement with the value for bulk solid fluoroalkane phases,<sup>43</sup> and the interfacial roughness is in agreement with the value calculated from our measured value of interfacial tension. This analysis shows that the monolayer at temperatures well below the phase transition is in a solid phase with all-trans molecules aligned nearly perpendicular to the interface.<sup>20</sup>

The solid lines in Figure 5a for the other temperatures are determined by analyzing the reflectivity data using one fitting parameter, the domain coverage  $C$  (see eqs 6 and 7). The success of this one parameter analysis indicates that at these other temperatures the monolayer consists of solid phase domains (whose structure is essentially the same as for the low-temperature homogeneous monolayer) separated by regions of gaseous monolayer. In contrast to the C<sub>20</sub>OH system, the gaseous monolayer could be described by a simple interface between hexane and water without the need for an intrinsic roughness,  $\sigma_o$  (and, therefore,  $\sigma_{\text{gas}}^2 = \sigma_{\text{cap}}^2$  in eq 5). This indicates that the

gas phase in the single surfactant FC<sub>10</sub>OH system contains very few FC<sub>10</sub>OH molecules. The layer thickness and electron density for the solid phase domains are determined by the fit to the data measured at  $T = 18$  °C (Table 3). The temperature dependence of the interfacial roughness  $\sigma$  is calculated from the variation of our measured values of the interfacial tension using the expression for  $\sigma_{\text{cap}}$  in eq 5.<sup>20</sup>

Figure 5b shows the domain coverage  $C$  determined by these one parameter fits to the data.<sup>20</sup> Note that in addition to the data shown in Figure 5a,  $R/R_F$  at four values of  $Q_z$  ( $=0.1, 0.15, 0.2,$  and  $0.25 \text{ \AA}^{-1}$ ) was measured for intermediate temperatures and used to produce values of the domain coverage.<sup>20</sup> Below the transition the interface is fully covered by an FC<sub>10</sub>OH monolayer. Above the transition the coverage decays gradually over a range of 30 °C. An earlier analysis of these data provided different coverage values depending upon whether the reflectivity was analyzed as coherent or incoherent (see eqs 6 and 7).<sup>20</sup> However, comparison with values of interfacial coverage calculated from the interfacial density determined from tension measurements (see Figure 5b) demonstrates that the analysis using coherent reflectivity is correct<sup>21</sup> (the coverage was calculated from the density by normalizing to the low-temperature value of the density,  $5.58 \mu\text{M/m}^2$ , a value that is consistent with the interfacial density expected for a fully covered interface<sup>27,43,45</sup>). This analysis provides strong support for the existence of domains above the phase transition because these data require the existence of regions of the interface that produce different reflected X-ray fields that interfere coherently. For a slightly longer surfactant, FC<sub>12</sub>OH ( $\text{CF}_3(\text{CF}_2)_9(\text{CH}_2)_2\text{OH}$ ), earlier X-ray diffuse scattering measurements provided direct evidence for the presence of domains of solid phases separated by gaseous regions of the monolayer.<sup>46</sup>

*Overview of the Analysis of Mixed Surfactant Monolayers.* The analysis of the X-ray reflectivity data from mixed surfactant monolayers poses several challenges. The expression for the reflectivity in eq 1 indicates that the reflected intensity depends on the electron density averaged over the  $x$ - $y$  plane of the interface. If the interface is homogeneous, i.e., the molecular arrangement is essentially the same for different  $x$ - $y$  positions on the interface, then the electron density profile (normal to the interface, along  $z$ ) produced by the analysis of the reflectivity data can often be simply related to molecular ordering normal to the interface. As will be discussed, phases 1 and 2 (see Figure 2) are homogeneous, single surfactant monolayers consisting of C<sub>20</sub>OH and FC<sub>10</sub>OH fully covering the interface. However, if the interface is heterogeneously covered by surfactants, then the analysis is not as straightforward.

As shown for single surfactant systems, the interface may contain domains of condensed phases separated by regions of a dilute gaseous monolayer. The analysis of data from systems with two surfactants is more complex because there can be more than one type of condensed domain as well as the possibility

**TABLE 3: Fitting Parameters for Homogeneous Monolayer Models<sup>a</sup>**

systems	$T$ (°C)	$\gamma$ ( $\pm 0.05$ ) ( $10^{-3}$ N/m)	$\sigma$ (Å)	$\sigma_{\text{cap}}$ (Å)	$L_h$ (Å)	layer 1		layer 2	
						$\rho_h$	$\rho_{\text{max}}$	$L_t$ (Å)	$\rho_t$
C <sub>20</sub> OH	19.38	22.9	4.7 <sup>+0.3/-1</sup>	4.70	8 <sup>±5</sup>	1.15 <sup>+1/-0.1</sup>	1.07 $\pm$ 0.02	17 $\pm$ 1.5	0.80 <sup>+0.01/-0.02</sup>
FC <sub>10</sub> OH	22.85	37.0	3.6 $\pm$ 0.3	3.76				10 $\pm$ 1	1.85 $\pm$ 0.09
B	15.88	26.6	N/A	4.51	7 $\pm$ 1	1.20 $\pm$ 0.04	1.09 $\pm$ 0.02	16.6 $\pm$ 0.15	0.812 $\pm$ 0.004
A	24.91	32.0	N/A	3.82				9.8 $\pm$ 0.2	1.904 $\pm$ 0.008

<sup>a</sup>  $T$  is the temperature;  $\gamma$  is the interfacial tension;  $\sigma$  is the fit roughness;  $\sigma_{\text{cap}}$  is the roughness calculated from the measured interfacial tension using capillary wave theory. Layers are ordered as water–headgroup (layer 1)—tailgroup (layer 2)—hexane.  $L$  is the layer thickness;  $\rho$  is the electron density normalized to the value of bulk water at the temperature for the measurement (e.g., 0.3337 e<sup>-</sup>/Å<sup>3</sup> at  $T = 20$  °C), normalized hexane density is 0.68 at  $T = 20$  °C. For the headgroup the maximum electron density and the density of the layer are given because the density and layer thickness fitting parameters are strongly correlated for this thin layer, but the resultant profile is well determined.<sup>21-54</sup> Systems A and B are illustrated in Figure 6c,a, respectively.

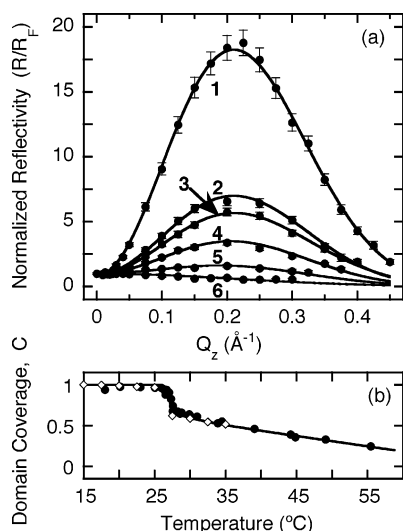


**Figure 5.** (a) X-ray reflectivity normalized to the Fresnel reflectivity from the interface between water and a 5.0 mmol/kg solution of FC<sub>10</sub>-OH in hexane: (1) 18.0 °C, (2) 27.9 °C, (3) 30.1 °C, (4) 36.5 °C, (5) 46.0 °C, (6) 55.5 °C. (b) Domain coverage as a function of temperature determined by the data in part a using coherent reflectivity as in eq 7. Dots are coverage determined from the X-ray measurements; diamonds are determined from analysis of tension measurements.<sup>20,44</sup> The solid line is a fit to a theory described elsewhere.<sup>20</sup>

of surfactant mixing within domains. As will be discussed, the data very near the phase transitions and the data in phase 3 cannot be adequately fit by a homogeneous monolayer. Although scattering from the bulk liquids has precluded the use of X-ray surface diffuse scattering to demonstrate directly the existence of domains, we will assume that the interface contains domains except where the analysis indicates a homogeneous interface fully covered by one of the two surfactants. Also, there are good theoretical reasons to expect that domains will be stabilized in systems containing surfactants with electric dipole moments.<sup>47-49</sup> Furthermore, we will assume that each of the domains contains a single kind of surfactant. This is plausible considering that fluorocarbons and hydrocarbons of this length typically do not mix in a bulk solution near room temperature (of just the two components, i.e., without hexane and water).<sup>9,50</sup> Our final assumption is that FC<sub>10</sub>OH domains have the same layer thicknesses and layer electron densities as for the homogeneous FC<sub>10</sub>OH monolayer phase, likewise for the C<sub>20</sub>OH. This last assumption is consistent with the results of our studies of the single surfactant systems. The only fitting parameters for the heterogeneous monolayers are the fraction of interface covered by each domain (one or two fitting parameters depending upon whether there are two or three different types of domains) and the interfacial roughness. We expect the latter to vary with temperature because the interfacial tension varies with temper-

ature. Although we have had to make strong assumptions to analyze these data, we consider them justified in light of our ability to use just two or three parameters to fit data from several different monolayer phases over large ranges in temperature for several different bulk concentrations.

An additional challenge in the analysis of these data is our ignorance of the size of domains in relation to the in-plane spatial coherence length of the X-rays (the latter is approximately 5  $\mu\text{m}$  for our measurements). If the domains are much smaller than this coherence length, then X-rays scattered from a domain and surrounding regions will add nearly coherently (i.e., the scattered electromagnetic fields add). If the domains are much larger than the coherence length, the scattered X-rays from neighboring domains add nearly incoherently (i.e., scattered intensities add). Although identifying the reflectivity as either coherent or incoherent provides some guide as to the domain size, it is not definitive. For example, it is possible that very large condensed phases that nearly fill the interface and are separated by thin regions of gas (whose width is less than the coherence length) would also be fit better by coherent reflectivity. With this caveat in mind, we will identify domains as smaller or larger than 5  $\mu\text{m}$  if the reflectivity is coherent or incoherent, respectively. Analysis of scattering from domains whose size is similar to the coherence length may involve more sophisticated theories of partial coherence.<sup>51</sup> We have assumed that the reflectivity can be modeled as due to either fully incoherent or coherent scattering as in eqs 6 and 7. Often, these data can be fit by both the incoherent or coherent models, but the fits may yield different values of the domain coverage for the two choices. In this case, consistency with our thermodynamic determination of the total interfacial density can determine the correct choice between the two types of reflectivity.

*Examples of Reflectivity Curves.* In this section, examples of reflectivity measurements at specific temperatures are discussed to illustrate our ability to discriminate between different models of the interfacial structure. These models describe either a homogeneous monolayer of a single surfactant that fully covers the interface or a heterogeneous monolayer consisting of domains. Three different types of domains may be present on the interface. These include gaseous domains, FC<sub>10</sub>OH domains (labeled as F domains), and C<sub>20</sub>OH domains (labeled as H domains). In addition, these domains may produce either coherent or incoherent reflectivity.

(a) *Homogeneous Monolayers.* Normalized X-ray reflectivity curves ( $R/R_F$ ) for system B at 15.88 °C (in phase 1) and for system A at 24.91 °C (in phase 2) are plotted in panels a and c of Figure 6. The line in panel a is a fit to a two-layer interface whose values of electron density and thickness for each layer are consistent with measurements of a homogeneous monolayer of C<sub>20</sub>OH that fully covers the water–hexane interface (compare

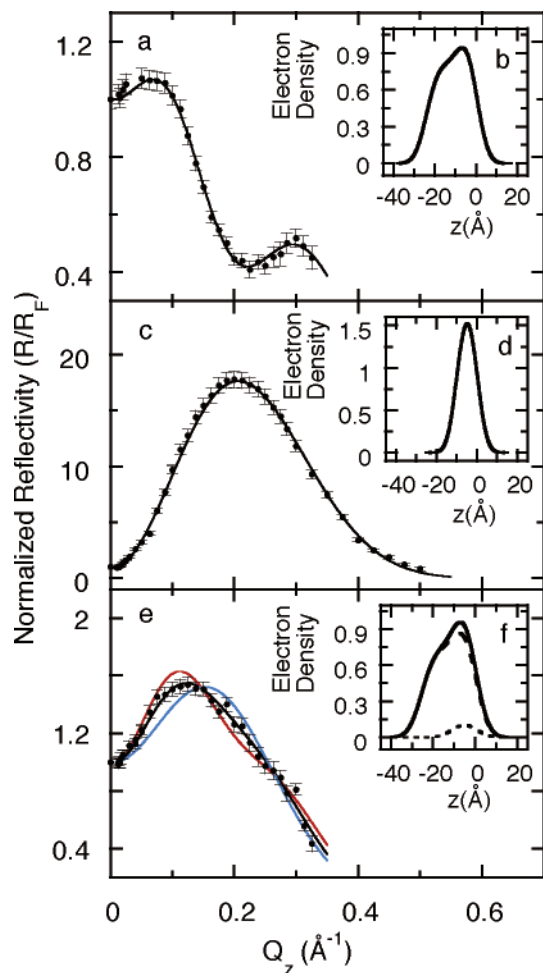


**Figure 6.** (a, c, e) Normalized reflectivity  $R/R_F$  vs wave vector transfer  $Q_z$  for mixed surfactant monolayers at the hexane–water interface. Data points (●). (b), (d), and (f) are the electron density profiles of the surfactant monolayer determined from the fits in (a), (c), and (e). The bulk water electron density ( $z > 0$ ) and the bulk hexane electron density ( $z \ll 0$ ) have been subtracted. (a) and (b) system B at 15.88 °C is fit by a homogeneous monolayer of  $C_{20}OH$  (phase 1; see Table 3). (c) and (d) system A at 24.91 °C is fit by a homogeneous monolayer of  $FC_{10}OH$  (phase 2; see Table 3). (e) System A at 21.97 °C (at the transition between phases 1 and 2) is fit by a two-domain ( $C_{20}OH$  and  $FC_{10}OH$ ) incoherent model (solid black line; see Table 4). Other models shown do not fit the data well: two-domain ( $C_{20}OH$  and  $FC_{10}OH$ ) coherent fit (red solid line); blue solid line represents three different fits—the homogeneous monolayer and two-domain incoherent and coherent fits of  $FC_{10}OH$  and gas domains. (f) Monolayer electron density profile obtained from the two-domain incoherent model:  $FC_{10}OH$  molecules (short dash),  $C_{20}OH$  molecules (long dash), and sum of both molecules (solid line).

to low-temperature data for the single surfactant system in Figure 4 and compare parameters in Table 3).<sup>21</sup>

The line in panel c is a fit to a one layer interface (compare to low temperature data for the single surfactant system in Figure 5). The parameters for the fit in panel c agree with the parameters from a water–hexane interface fully covered by  $FC_{10}OH$  (compare parameters for single and mixed surfactant systems in Table 3).<sup>20</sup>

Panels b and d of Figure 6 illustrate the electron density profile normal to the interface. In these figures the electron density due to the bulk water and hexane solution has been subtracted to illustrate the electron density of the surfactant layer. The profiles in the figures are rounded due to the capillary wave roughening of the interfaces. Extra electron density in the headgroup region can be seen for  $C_{20}OH$  in Figure 6b.

Comparison of the two figures shows the much larger electron density of the  $FC_{10}OH$  layer.

(b) Two-Domain Models. Figure 6e illustrates reflectivity data from system A at 21.97 °C (at the transition between phases 1 and 2). Although these data have a single maximum, the amplitude is not large enough to represent an interface fully covered by a layer of  $FC_{10}OH$  molecules as in Figure 6c. Also, the shape of the peak in Figure 6e is not similar to those in panels a and c of Figure 6, indicating that these data cannot be fit by domains of  $FC_{10}OH$  surrounded by regions of gaseous monolayer or by domains of  $C_{20}OH$  surrounded by gas. Quantitative fitting is consistent with these qualitative observations. The only good fit to the data in Figure 6e was obtained by a model that included separate domains of  $FC_{10}OH$  and  $C_{20}OH$ . In this model the molecular structure parameters (layer thickness and electron density) of the domains are fixed to the values used for the homogeneous monolayer fits (Table 3). The only fitting parameters for the two-domain models are the interfacial roughness and coverage of the domains (see eqs 6 and 7). Both coherent and incoherent two-domain models were tried; however, only the incoherent model fit the data (as illustrated in Figure 6e). This reveals the presence of domains larger than  $\sim 5 \mu m$  for system A at this temperature. The fit indicates that 8% of the interface is covered by  $FC_{10}OH$  with the rest covered by domains of  $C_{20}OH$  (see Table 4). Figure 6f illustrates the total surfactant electron density profile at the interface as well as separate profiles for  $FC_{10}OH$  and  $C_{20}OH$ .

Figure 7a illustrates reflectivity data for a monolayer with a large fraction of the interface covered by  $FC_{10}OH$  (system A at 26.88 °C, at the phase transition between phases 2 and 3). Although the form of the reflectivity is similar to Figure 6c, the amplitude is smaller, indicating that part of the interface is covered by  $C_{20}OH$  or gas. These data are similar to data in Figure 5 from the single surfactant  $FC_{10}OH$  system near or above the phase transition.

These data were fit by two-domain models, both coherent and incoherent, that include  $FC_{10}OH$  domains with either  $C_{20}OH$  or gaseous domains. Figure 7a illustrates that all four fits are nearly indistinguishable. In addition, a three domain model can also fit these data. Table 4 shows that the coverage of the  $FC_{10}OH$  domains determined by the different fits varies from 85% to 93% with the remainder of the interface covered by  $C_{20}OH$  and/or gaseous domains.

Because the reflectivity from a fully covered  $FC_{10}OH$  interface is much larger than that from a fully covered  $C_{20}OH$  interface or from the water–hexane interface, it is difficult to determine the fraction of these other domains when the interface is covered primarily by  $FC_{10}OH$ . In this particular case it is also difficult to distinguish between coherent and incoherent reflectivity.

Normalized reflectivity data for system B at 25.04 °C (in phase 3) are shown in Figure 7b. Three domains are required to fit these data. These fits have three fitting parameters: the interfacial roughness and two values of coverage ( $C_F$  and  $C_H$ ) for the  $FC_{10}OH$  and  $C_{20}OH$  domains. The coverage for the gaseous region that fills up the remainder of the interface is given by  $1 - C_H - C_F$ . Coverage values and the interfacial roughness are listed in Table 4. Both coherent and incoherent reflectivity can be used to fit these data though they yield very different coverage values. As discussed later, thermodynamic measurements for the interfacial density can determine whether the coherent or incoherent model is correct.

*Full Reflectivity Curves.* The complete reflectivity measurements for systems A–D are illustrated in Figures 8–11.

**TABLE 4: Fitting Parameters for Multiple Domain Models<sup>a</sup>**

system	$T$ (°C)	$\gamma$ ( $\pm 0.05$ ) ( $10^{-3}$ N/m)	model	$\sigma_{\text{cap}}$ (Å)	$\sigma$ (Å)	$C_{\text{H}}$	$C_{\text{F}}$	$C_{\text{G}}$
Two-Domain Fits								
A	21.97	25.5	inc (H, F)	4.66	$4.91 \pm 0.07$	$0.92 \pm 0.005$	$0.08 \pm 0.005$	0
A	26.88	34.5	inc (H, F)	4.09	$4.13 \pm 0.06$	$0.16 \pm 0.035$	$0.84 \pm 0.035$	0
A	26.88	34.5	inc (F, G)	4.09	$4.12 \pm 0.06$	0	$0.85 \pm 0.035$	$0.15 \pm 0.035$
A	26.88	34.5	coh (H, F)	4.09	$4.14 \pm 0.06$	$0.10 \pm 0.025$	$0.90 \pm 0.025$	0
A	26.88	34.5	coh (F, G)	4.09	$4.13 \pm 0.06$	0	$0.93 \pm 0.015$	$0.07 \pm 0.015$
Three-Domain Fits								
B	25.04	40.2	inc	3.75	4.48	$0.48 \pm 0.12$	$0.11 \pm 0.03$	$0.41 \pm 0.12$
B	25.04	40.2	coh	3.75	4.45	$0.32 \pm 0.07$	$0.35 \pm 0.02$	$0.33 \pm 0.05$

<sup>a</sup> Model refers to the use of either incoherent (inc) or coherent (coh) reflectivity;  $\sigma$  is the roughness of the  $\text{C}_{20}\text{OH}$  and  $\text{FC}_{10}\text{OH}$  domains (the roughness of the gas domains was fixed at 5.5 Å);  $C_{\text{H}}$ ,  $C_{\text{F}}$ , and  $C_{\text{G}}$  are the interfacial domain coverages of  $\text{C}_{20}\text{OH}$ ,  $\text{FC}_{10}\text{OH}$ , and gas domains, respectively; two-domain fits are either  $\text{C}_{20}\text{OH}$  and  $\text{FC}_{10}\text{OH}$  domains (H, F) or  $\text{FC}_{10}\text{OH}$  and gas domains (F, G); three-domain fits are  $\text{C}_{20}\text{OH}$ ,  $\text{FC}_{10}\text{OH}$ , and gas domains. System A (21.97 °C) is illustrated in Figure 6e; system A (26.88 °C) is illustrated in Figure 7a; system B (25.04 °C) is illustrated in Figure 7b.

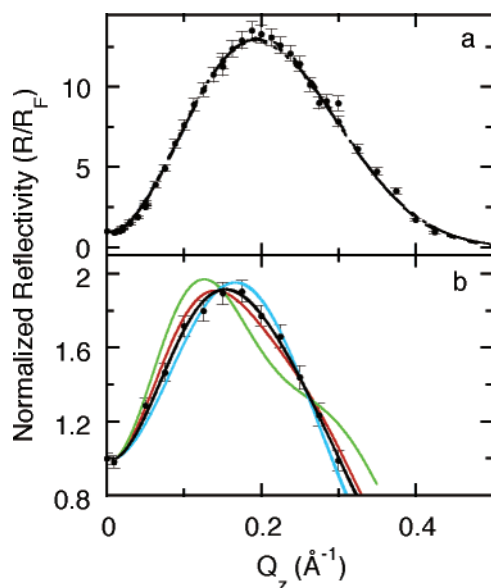


**Figure 7.** Normalized reflectivity  $R/R_{\text{F}}$  vs wave vector transfer  $Q_z$  for mixed surfactant monolayers at hexane–water interface. (a) System A at 26.88 °C (near the transition between phases 2 and 3; see also Table 4). Nearly overlapping lines represent seven different fits as described in text. (b) System B at 25.04 °C (in phase 3) is well fit by the three domain incoherent and coherent models (solid black line; see also Table 4). Other models do not fit the data properly. These consist of incoherent reflectivity from  $\text{C}_{20}\text{OH}/\text{FC}_{10}\text{OH}$  domains (red solid line), two-domain coherent model of  $\text{C}_{20}\text{OH}/\text{FC}_{10}\text{OH}$  domains (green solid line), and two-domain incoherent and coherent models of  $\text{FC}_{10}\text{OH}/\text{gas}$  domains (blue solid line).

Inspection shows many similarities with the example reflectivity curves just discussed in detail. The lines in these figures are examples of best fits; however, considerations similar to those used for the analysis of the example reflectivity curves were used to analyze all the reflectivity measurements.

**Interfacial Density.** The interfacial density of  $\text{FC}_{10}\text{OH}$  and  $\text{C}_{20}\text{OH}$  can be determined from the electron density profiles derived from the X-ray reflectivity data in Figures 8–11. Integration over the  $z$ -coordinate of electron density profiles for a homogeneous monolayer as shown, e.g., in panels b and d of Figure 6 will yield the number of electrons per unit area in the plane of the interface. Dividing this number by the number of electrons per  $\text{FC}_{10}\text{OH}$  (or  $\text{C}_{20}\text{OH}$ ) molecule yields the number of molecules of  $\text{FC}_{10}\text{OH}$  (or  $\text{C}_{20}\text{OH}$ ) per area of the interface. This is then converted into an interfacial density in  $\text{mol}/\text{m}^2$ .

For heterogeneous monolayers a similar procedure is followed except that the partial electron density corresponding to either  $\text{FC}_{10}\text{OH}$  or  $\text{C}_{20}\text{OH}$  molecules (as in Figure 6f) is used to

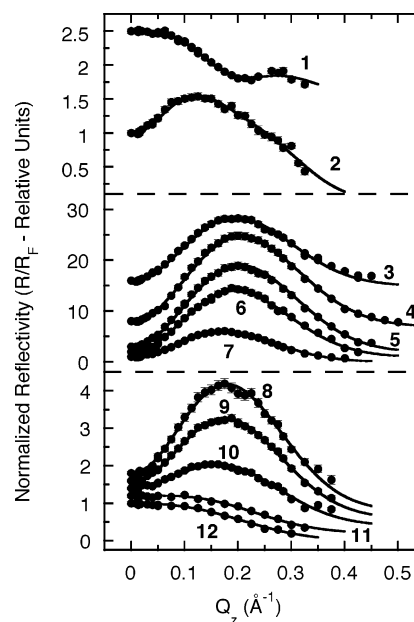


**Figure 8.** Normalized reflectivity for system A: (1)  $21.09 \pm 0.01$  °C, (2)  $21.97 \pm 0.01$  °C, (3)  $23.88 \pm 0.01$  °C, (4)  $24.91 \pm 0.02$  °C, (5)  $25.88 \pm 0.02$  °C, (6)  $26.88 \pm 0.02$  °C, (7)  $27.99 \pm 0.01$  °C, (8)  $28.89 \pm 0.01$  °C, (9)  $30.92 \pm 0.02$  °C, (10)  $36.42 \pm 0.01$  °C, (11)  $52.18 \pm 0.01$  °C, (12)  $57.71 \pm 0.01$  °C. Data shifted for clarity ( $R/R_{\text{F}} = 1$  at  $Q_z = 0$  before shifting). Lines are fits described in the text.

determine the interfacial density of those molecules. If both  $\text{FC}_{10}\text{OH}$  and  $\text{C}_{20}\text{OH}$  domains exist, then the total interfacial density can be determined by the sum of the individual densities. Gaseous regions may also be present, but the X-ray reflectivity is not sensitive to the number of  $\text{FC}_{10}\text{OH}$  or  $\text{C}_{20}\text{OH}$  molecules in this lower density phase. In this case, the total interfacial density determined from the X-ray measurements will underestimate the real density of  $\text{FC}_{10}\text{OH}$  and  $\text{C}_{20}\text{OH}$  molecules at the interface.

The domain coverage,  $C$  (fraction of interface covered by domains of  $\text{FC}_{10}\text{OH}$  or  $\text{C}_{20}\text{OH}$ ), can also be determined using our earlier assumption that the domains consist of  $\text{FC}_{10}\text{OH}$  or  $\text{C}_{20}\text{OH}$  molecules in a condensed phase similar to that in the homogeneous phases. Note that our domain coverage,  $C$ , is different from the standard thermodynamic coverage (typically referred to as  $\theta$ ). The coverage  $\theta$  refers to the total number of surfactant molecules at the interface normalized by the number of surfactant molecules in a fully covered, close-packed monolayer. X-ray reflectivity cannot determine the number of surfactant molecules in the low-density gas phase. Therefore, the two coverages  $\theta$  and  $C$  will be slightly different.

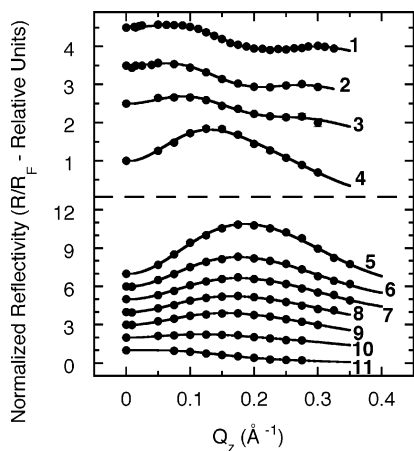


**Figure 9.** Normalized reflectivity for system B: (1)  $15.88 \pm 0.03$  °C, (2)  $17.97 \pm 0.02$  °C, (3)  $19.89 \pm 0.01$  °C, (4)  $20.17 \pm 0.02$  °C, (5)  $20.68 \pm 0.02$  °C, (6)  $21.17 \pm 0.02$  °C, (7)  $21.67 \pm 0.02$  °C, (8)  $22.78 \pm 0.02$  °C, (9)  $25.04 \pm 0.01$  °C, (10)  $31.95 \pm 0.01$  °C, (11)  $55.9 \pm 0.01$  °C. Data shifted for clarity ( $R/R_F = 1$  at  $Q_z = 0$  before shifting). Lines are fits described in the text.

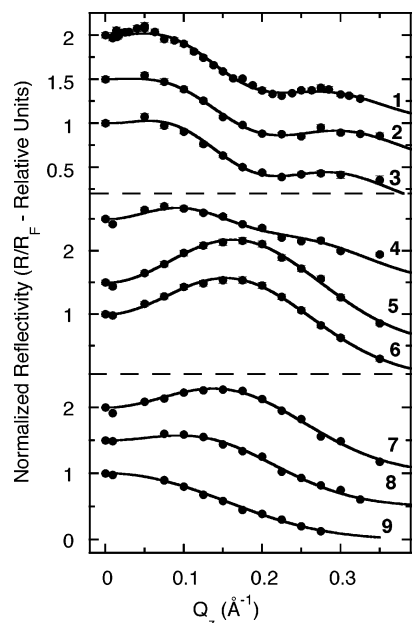


**Figure 10.** Normalized reflectivity for system C: (1)  $18.06 \pm 0.02$  °C, (2)  $19.89 \pm 0.02$  °C, (3)  $20.96 \pm 0.02$  °C, (4)  $21.53 \pm 0.02$  °C, (5)  $22.97 \pm 0.02$  °C, (6)  $23.97 \pm 0.02$  °C, (7)  $25.00 \pm 0.02$  °C, (8)  $32.08 \pm 0.02$  °C, (9)  $57.32 \pm 0.02$  °C. Data shifted for clarity ( $R/R_F = 1$  at  $Q_z = 0$  before shifting). Lines are fits described in the text.

The interfacial density and domain coverage for systems A–D are shown in Figures 12–15 (corresponding to the data in Figures 8–11). Results from all the interfacial models that adequately fit the data are presented. However, comparison with the thermodynamically derived interfacial density will allow us to reject many of the models.

**System A.** At the lowest temperature the monolayer is in phase 1 (Figure 12). This is a homogeneous close-packed  $C_{20}OH$  monolayer, as indicated by a coverage of one for  $C_{20}OH$  in panel b and zero for  $FC_{10}OH$  in panel c of Figure 12. At temperatures slightly above 23 °C the coverage of  $FC_{10}OH$  rapidly rises to one and the coverage of  $C_{20}OH$  rapidly falls to zero. The interface has passed through a phase transition to a homogeneous close-packed  $FC_{10}OH$  monolayer known as phase 2. During the transition the interface contains domains of both  $C_{20}OH$  and  $FC_{10}OH$ .

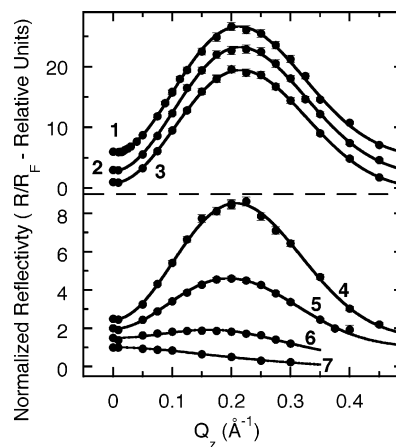


**Figure 11.** Normalized reflectivity for system D: (1)  $18.92 \pm 0.04$  °C, (2)  $21.89 \pm 0.05$  °C, (3)  $23.39 \pm 0.05$  °C, (4)  $25.02 \pm 0.04$  °C, (5)  $30.57 \pm 0.03$  °C, (6)  $40.52 \pm 0.01$  °C, (7)  $55.40 \pm 0.02$  °C. Data shifted for clarity ( $R/R_F = 1$  at  $Q_z = 0$  before shifting). Lines are fits described in the text.

At approximately 27 °C the interface passes through another transition to phase 3 at which the  $FC_{10}OH$  coverage drops quickly though the  $C_{20}OH$  coverage remains at a low value. Above 27 °C, the coverage of  $FC_{10}OH$  decreases slowly with temperature, similarly to the coverage of the single surfactant  $FC_{10}OH$  system shown in Figure 5. The data above 27 °C are consistent with the presence of either  $FC_{10}OH$  domains separated by regions of gas or both  $FC_{10}OH$  and  $C_{20}OH$  domains separated by regions of gas. In the latter case the coverage of  $C_{20}OH$  domains in phase 3 is always within error bars of zero.

The two sets of values in phase 3, shown in panels a and c of Figure 12, are due to the difference between coherent and incoherent reflectivity. In both cases the data are fit well, but the determination of the interfacial density is different. This ambiguity can be resolved by comparison with the total interfacial density determined by the interfacial tension measurements (the diamonds in Figure 12a). This thermodynamic density is consistent only with the coherent model for the X-ray reflectivity. In addition, nonmonotonic behavior of the density produced by the three-domain models above 27 °C leads us to discard these models. Therefore, phase 3 consists of  $FC_{10}OH$  domains (smaller than 5  $\mu m$ ) separated by regions of gas, although the possibility of the presence of a small fraction of  $C_{20}OH$  domains cannot be eliminated.

**System B.** The interfacial density and domain coverage for system B are shown in Figure 13. Note that systems A and B have the same composition ratio, but the choice of total surfactant concentration,  $m$ , determines that system B exhibits only one phase transition (see Figure 2a).

Similar to Figure 12, at the lowest temperatures in Figure 13 the monolayer is in phase 1, a homogeneous close-packed  $C_{20}OH$  monolayer. Very close to the phase transition ( $T \approx 20.5$  °C) both  $FC_{10}OH$  and  $C_{20}OH$  domains are present on the surface (without gaseous regions). Above the transition to phase 3, only three-domain models with  $FC_{10}OH$  and  $C_{20}OH$  domains plus gas regions fit the data. Comparison with the total interfacial density determined by the tension measurements (see diamonds in Figure 13a) indicate that above the transition the incoherent reflectivity model (green squares) is correct.

Figures 12 and 13 show that the total interfacial density of surfactants in phase 3 is larger in system A, which has a larger total bulk concentration  $m$ . The ratio of interfacial coverage of  $FC_{10}OH$  to the total surfactant coverage (Figure 13d) in phase 3 is also different for systems A and B, being essentially 1 for

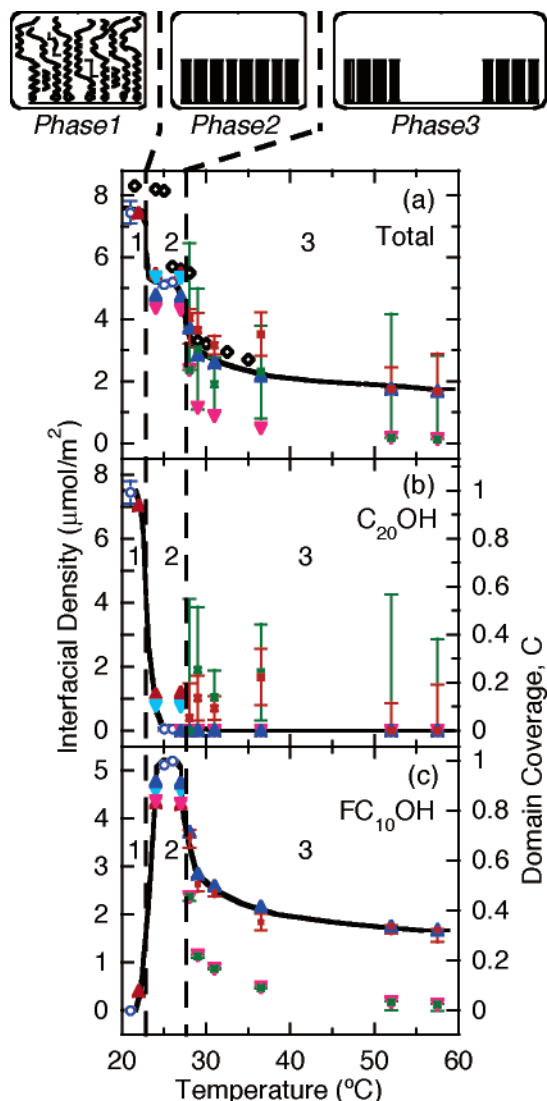


**Figure 12.** System A ( $X_2 = 0.280$ ,  $m = 25.06$  mmol/kg): (a) total for  $\text{FC}_{10}\text{OH}$  and  $\text{C}_{20}\text{OH}$ ; (b)  $\text{C}_{20}\text{OH}$  only; (c)  $\text{FC}_{10}\text{OH}$  only. Interfacial density of surfactants vs temperature. Cartoons of the phases, for illustrative purposes only, are shown above panel a. The solid lines in panels a–c indicate the correct model determined by considering results of both X-ray and tension measurements. Vertical dashed lines separate phases 1–3. For panels b and c, the right axis shows the domain coverage for  $\text{C}_{20}\text{OH}$  and  $\text{FC}_{10}\text{OH}$  that corresponds to the density. Legend: thermodynamic measurement ( $\diamond$ ). Other symbols for X-ray reflectivity: blue circle, homogeneous monolayer model;  $\text{C}_{20}\text{OH}$  and  $\text{FC}_{10}\text{OH}$  domains: dark-red up-triangle, two-domain incoherent model; light-blue down-triangle, two-domain coherent model.  $\text{FC}_{10}\text{OH}$  and gas domains: pink down-triangle, two-domain incoherent model; blue up-triangle, two-domain coherent model. Three domains ( $\text{C}_{20}\text{OH}$ ,  $\text{FC}_{10}\text{OH}$ , and gas): green square, incoherent model; red square, coherent model.

system A, but much less than 1 for system B even though the bulk concentration ratio  $X_2 = 0.28$  for both systems.

This is an indication of the nonideality of these solutions previously discussed in the literature.<sup>17</sup> In addition, the reflectivity in phase 3 for system A is coherent whereas in system B it is incoherent. This indicates that the pattern of domains has evolved in passing from system A to system B. This is likely due to the presence of  $\text{C}_{20}\text{OH}$  domains in phase 3 of system B. These occupy 10–20% of the interface for system B but are absent in system A.

**System C.** The interfacial density and domain coverage for system C are shown in Figure 14. Figure 2b indicates that only

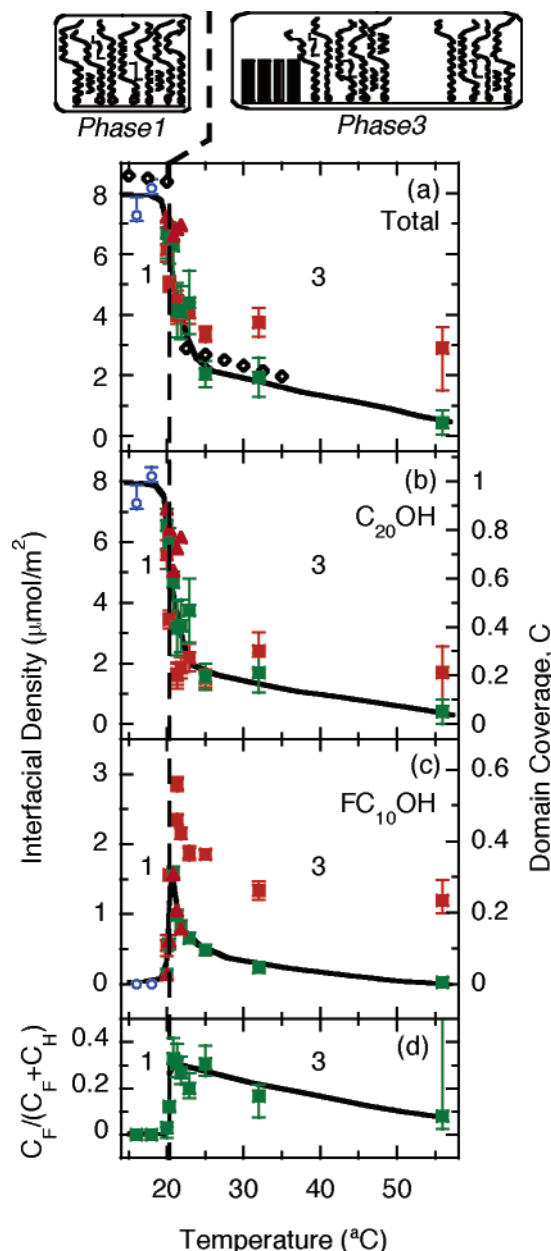


**Figure 13.** System B ( $X_2 = 0.280$ ,  $m = 12.46$  mmol/kg): (a) total for  $\text{FC}_{10}\text{OH}$  and  $\text{C}_{20}\text{OH}$ , (b)  $\text{C}_{20}\text{OH}$  only, (c)  $\text{FC}_{10}\text{OH}$  only. (d) Ratio of  $\text{FC}_{10}\text{OH}$  coverage to total surfactant coverage. Interfacial density of surfactants vs temperature. Cartoons of the phases, for illustrative purposes only, are shown above panel a. The solid lines in panels a–c indicate the correct model determined by considering results of both X-ray and tension measurements. Vertical dashed line separates phases 1 and 3. For panels b and c, the right axis shows the domain coverage for  $\text{C}_{20}\text{OH}$  and  $\text{FC}_{10}\text{OH}$  that corresponds to the density. Legend as in Figure 12.

one phase transition is present. Again, the low-temperature phase 1 is a homogeneous close-packed  $\text{C}_{20}\text{OH}$  monolayer. Comparison with the thermodynamic determination of the density indicates that the coherent model is correct above the transition at  $T \approx 22$  °C to phase 3. As in Figure 12 the three-domain models are rejected because of the nonmonotonic behavior of the density in phase 3. In phase 3 these considerations indicate that the two-domain coherent model of  $\text{FC}_{10}\text{OH}$  domains separated by gaseous regions is correct (blue triangles). This is similar to phase 3 of system A.

**System D.** The interfacial density and domain coverage for system D are shown in Figure 15. Figure 2c indicates that only

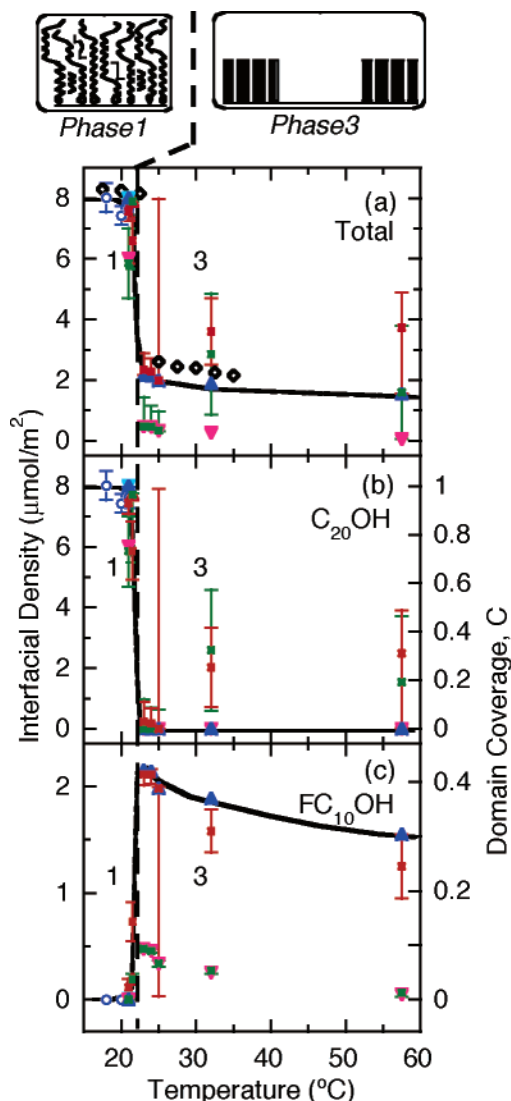


**Figure 14.** System C ( $X_2 = 0.250$ ,  $m = 15.00$  mmol/kg): (a) total for  $\text{FC}_{10}\text{OH}$  and  $\text{C}_{20}\text{OH}$ , (b)  $\text{C}_{20}\text{OH}$  only, (c)  $\text{FC}_{10}\text{OH}$  only. Interfacial density of surfactants vs temperature. Cartoons of the phases, for illustrative purposes only, are shown above panel a. The solid lines in panels a–c indicate the correct model determined by considering results of both X-ray and tension measurements. Vertical dashed line separates phases 1 and 3. For panels b and c, the right axis shows the domain coverage for  $\text{C}_{20}\text{OH}$  and  $\text{FC}_{10}\text{OH}$  that corresponds to the density. Legend as in Figure 12.

one phase transition is present. In this system the low-temperature phase is a homogeneous close-packed  $\text{FC}_{10}\text{OH}$  monolayer, phase 2. This agrees with the determination by the interfacial excess entropy. Comparison with the thermodynamic determination of the density indicates that the coherent model is correct above the transition at  $T \approx 24$  °C to phase 3. The three-domain models are rejected because of the nonmonotonic behavior of the density in the high-temperature phase. In the high-temperature phase 3 these considerations indicate that the two-domain coherent model of  $\text{FC}_{10}\text{OH}$  domains separated by gaseous regions is correct (blue triangles). This is similar to phase 3 of systems A and C.

## Discussion

**Phase Diagram.** Figure 2 illustrates the phase diagrams for three different fractions of  $\text{FC}_{10}\text{OH}$  as given by  $X_2$ . For the two smaller fractions,  $X_2 = 0.25$  and  $0.28$ , the lowest temperature phase (phase 1) is a homogeneous monolayer of  $\text{C}_{20}\text{OH}$  with a

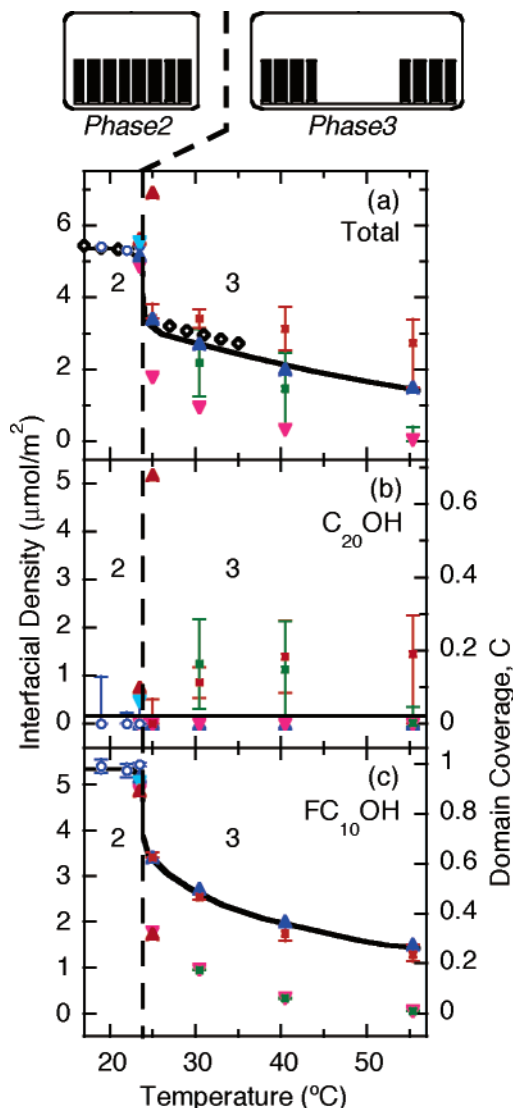


**Figure 15.** System D ( $X_2 = 0.500$ ,  $m = 8.802$  mmol/kg): (a) total for  $\text{FC}_{10}\text{OH}$  and  $\text{C}_{20}\text{OH}$ , (b)  $\text{C}_{20}\text{OH}$  only, (c)  $\text{FC}_{10}\text{OH}$  only. Interfacial density of surfactants vs temperature. Cartoons of the phases, for illustrative purposes only, are shown above panel a. The solid lines in panels a–c indicate the correct model determined by considering results of both X-ray and tension measurements. Vertical dashed line separates phases 2 and 3. For panels b and c, the right axis shows the domain coverage for  $\text{C}_{20}\text{OH}$  and  $\text{FC}_{10}\text{OH}$  that corresponds to the density. Legend as in Figure 12.

coverage of nearly 1. For the highest fraction of  $\text{FC}_{10}\text{OH}$ ,  $X_2 = 0.5$ , the low-temperature phase is a homogeneous monolayer of  $\text{FC}_{10}\text{OH}$  with a coverage of nearly 1. This phase 2 is also present for  $X_2 = 0.28$  at intermediate temperatures in system A. Because phase 1 is a liquid monolayer of  $\text{C}_{20}\text{OH}$  and phase 2 is a solid monolayer of  $\text{FC}_{10}\text{OH}$ , the phase sequence for system A has the unusual feature of progressing from a liquid to a solid monolayer with increasing temperature.

At the highest temperatures, in phase 3, the interface contains domains of  $\text{FC}_{10}\text{OH}$  with a coverage much less than 1 (approximately 0.3 to 0.4 for systems A, C, and D). Between the domains are gaseous regions of nearly pure water–hexane interface with a small number of alkanol molecules. For systems A, C, and D there may be a small number of  $\text{C}_{20}\text{OH}$  molecules in phase 3 that are below our detection limit. However, for system B up to 20% of the interface is covered with  $\text{C}_{20}\text{OH}$  domains with a smaller amount of the interface covered by  $\text{FC}_{10}\text{OH}$  domains (see Figure 13). The interfacial tension measure-

ments as a function of temperature do not indicate the presence of a phase transition within the region of phase 3, e.g., between the concentrations of systems A and B. Therefore, the variation of the amount of C<sub>20</sub>OH and FC<sub>10</sub>OH within phase 3 does not represent a phase transition, but rather a crossover. More data for different values of the concentration *m* are required to determine the dependence of the C<sub>20</sub>OH domain coverage in the region of phase 3.

Within phase 3, for systems A, C, and D (with essentially only FC<sub>10</sub>OH domains and gas), the reflectivity is coherent. This indicates that domains of FC<sub>10</sub>OH are smaller than the X-ray coherence length of  $\sim 5 \mu\text{m}$  in the plane of the interface. For system B, the reflectivity must be interpreted as incoherent. This may indicate that all the domains, both FC<sub>10</sub>OH and C<sub>20</sub>OH domains, are larger than the in-plane coherence length. Alternatively, it is possible that only the C<sub>20</sub>OH domains are larger than the coherence length whereas the FC<sub>10</sub>OH domains maintain their small size. A more detailed analysis of the X-ray coherence that includes partial coherence might be able to distinguish between these two possibilities. As discussed, reflectivity from the single surfactant FC<sub>10</sub>OH system is coherent and indicates that FC<sub>10</sub>OH prefers to form small domains. This is consistent with our results for the mixed system. Our analysis is also consistent with Brewster angle microscopy that shows C<sub>18</sub>OH at the water–hexane interface forms large domains and FC<sub>12</sub>OH at the water–hexane interface forms resolution-limited domains (i.e., smaller than  $10 \mu\text{m}$  for the microscopy measurements).<sup>52</sup>

**Phase Rule.** Phase 3 consists of domains of FC<sub>10</sub>OH and C<sub>20</sub>OH as well as gaseous regions between the domains. The Gibbs phase rule indicates that phase 3 is not a region of coexistence between interfacial phases, but rather that the interface is in a single phase that is spatially heterogeneous. This is a consequence of our observations that the domains are observed over a range of temperatures, that the domains are in equilibrium, and that the role of impurities seems to be negligible. To consider this in more detail, we state the phase rule for our system. The thermodynamic variance *w* is

$$w = 2 + (c - r) - \phi - (\psi - s) \quad (8)$$

where *c* = 4 is the number of components (water, hexane, FC<sub>10</sub>OH, and C<sub>20</sub>OH), *r* = 0 is the number of chemical reactions,  $\phi$  = 2 is the number of bulk phases, *s* = 1 is the number of types of surfaces, and  $\psi$  is the number of surface phases.<sup>53</sup> Equation 8 is appropriate for systems in which the surface phases are contiguous (so we only consider the liquid–liquid interface) and the surface is flat. For one-surface phase,  $\psi = 1$ , our system is tetravariant, *w* = 4, indicating that four intensive thermodynamic variables can be varied within a region of the phase diagram that contains the chosen surface phase. For our system, we take these four variables to be temperature, bulk pressure (1 atm), and the two concentrations *m* and *X*<sub>2</sub>. For two surface phases, our system is trivariant, *w* = 3, and two surface phases should exist only at one temperature for a chosen bulk pressure and alkanol concentrations *m* and *X*<sub>2</sub>. Three surface phases can exist only at one temperature and total surfactant concentration *m* for a chosen bulk pressure and concentration *X*<sub>2</sub>.

Because phases 1 and 2 are homogeneous, they represent a state of the interface with one surface phase. In this case the phase can exist over a range of temperatures (for a given pressure and concentrations *m* and *X*<sub>2</sub>) as shown in Figure 2. If we consider phase 3 of systems A, C, and D (with essentially only FC<sub>10</sub>OH domains and gas) to be a coexistence between two phases, then that coexistence should occur only at one

temperature. Similarly, if phase 3 of system B is considered to be a coexistence of three phases (FC<sub>10</sub>OH, C<sub>20</sub>OH, and gas phases), then it should exist at only one temperature and concentration *m*. However, phase 3 exists for a range of temperatures and concentrations.

Alternatively, domains can be the result of competing interactions that yield a single, spatially heterogeneous, surface phase.<sup>47,48</sup> In this case, the interfacial concentration is not isotropic but has variations within the interface that represent the domains. Because this spatially heterogeneous surface phase is a single surface phase, it can exist over a range of temperatures. A similar situation occurs with single surfactant alkanols at the water–hexane interface that exhibit domain phases.<sup>21</sup>

It is also possible that domains can appear over a range of temperatures due to the presence of impurities (an additional component) or nonequilibrium effects. Because alkanol molecules can freely exchange between the bulk and the interface, there is good reason to believe our systems are in, or very close, to equilibrium (as previously discussed in the literature<sup>46</sup>). In our earlier measurements of a single surfactant system using CF<sub>3</sub>(CF<sub>2</sub>)<sub>9</sub>(CH<sub>2</sub>)<sub>2</sub>OH monolayers at the water–hexane interface we tested the role of impurities. In those measurements, we showed that the presence of impurities may lead to hysteresis in the temperature of the phase transition upon heating or cooling the system, but that domains are always present even for systems with an impurity level low enough to eliminate the hysteresis. Although it is always possible that even a very small amount of impurities could stabilize the domains, we believe it is more likely that the phases we are observing are single, spatially heterogeneous phases.

If the phase transition lines in Figure 2 represent coexistence regions at a first-order phase transition, then, consistent with the phase rule, two surface phases exist just at the one temperature for a chosen bulk pressure and alkanol concentrations *m* and *X*<sub>2</sub>. Also consistent with the phase rule is the existence of the triple point for *X*<sub>2</sub> = 0.28 in which three surface phases can exist at a single temperature and concentration *m* for a chosen bulk pressure and concentration *X*<sub>2</sub>.

**Variation of Interfacial Density with Temperature.** *To a first approximation, the variation of domain coverage (or interfacial density) with temperature in this mixed system can be considered as a simple superposition of the behavior of the two single surfactant systems.* This superposition will be performed by using the relative values of the free energy of adsorption of the two surfactants to determine the fraction at the interface. This simple approach explains all the qualitative features of these data.

Panels a–d of Figure 16 illustrate the temperature dependence of the interfacial coverage for single surfactant systems of either FC<sub>10</sub>OH (concentration of 5.0 mmol/kg) or C<sub>20</sub>OH (15.0 mmol/kg), previously shown in Figures 4b and 5b. Panel b of Figure 16 is different because it illustrates the analysis using incoherent reflectivity for the single surfactant systems, whereas panels a, c, and d show the coherent reflectivity analysis. Although we have shown that the coherent analysis is correct for the single surfactant FC<sub>10</sub>OH system, we use the incoherent analysis as the basis for our discussion of the mixed system B because we have demonstrated that phase 3 of system B must be described by incoherent reflectivity.

The temperatures of the transitions for the two single surfactant systems have been shifted in panels a–d to indicate the correct transition temperatures for a single surfactant system with the same surfactant concentration as in the mixed systems

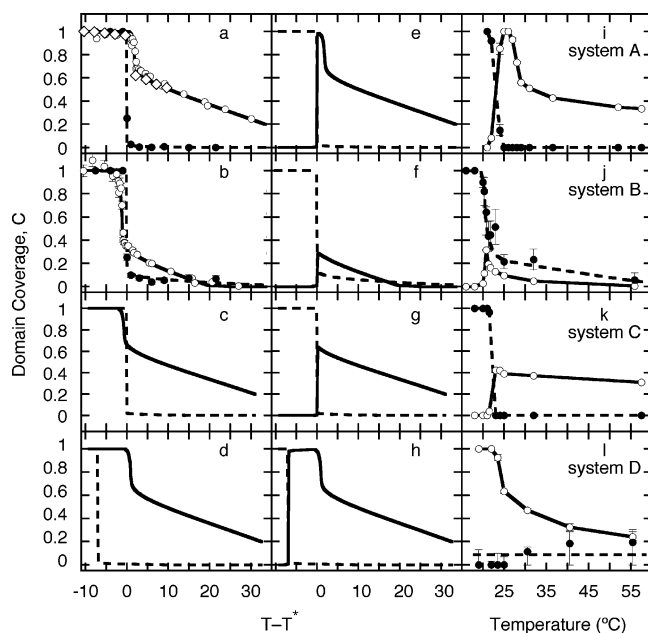


**Figure 16.** Domain coverage vs temperature. Rows represent systems A to D (top to bottom). (a)–(d) Results from studies of single surfactant  $C_{20}OH$  (dashed lines) and  $FC_{10}OH$  (solid lines) systems taken from Figures 4b and 5b. The curves have been shifted in temperature such that the transition temperatures,  $T^*$ , correspond to those of a single surfactant system whose concentration is the same as the concentration of that surfactant in the corresponding mixed system (Table 2). Panels a and b show the underlying data that allowed these curves to be derived (note that panel a has the same data as Figures 4b and 5b). Panel b has a different form because the data in Figure 13 show that system B is described by incoherent reflectivity, so we use an incoherent reflectivity analysis of the single surfactant systems to make a prediction for system B. Systems A, C, and D were well described by coherent reflectivity. (e)–(h) The second column is a weighted sum of the single surfactant  $C_{20}OH$  and  $FC_{10}OH$  systems depicted in the first column as described in the text. (i)–(l) The third column is the result obtained from the experiments performed on the mixed system (correct results extracted from Figures 12–15). Comparison of the second and third columns shows that the prediction from the behavior of the single surfactant systems correctly determines the qualitative features of the mixed system.

A–D. As shown in Figure 3 and listed in Table 2, we determined these transition temperatures by interfacial tension measurements. For example, the mixed system A contained a concentration of  $FC_{10}OH$  of  $m_F = 7.02$  mmol/kg and the transition temperature of a single surfactant  $FC_{10}OH$  system at that concentration is  $31$  °C (Table 2). Likewise, system A contained  $C_{20}OH$  at a concentration  $m_H = 18.04$  mmol/kg and the transition temperature of the corresponding single surfactant  $C_{20}OH$  system is  $29$  °C. Therefore, panel a of Figure 16 shows the domain coverage curves for the single surfactant systems of  $C_{20}OH$  and  $FC_{10}OH$  with the transition for  $FC_{10}OH$  higher by  $2$  °C. Similarly, panels (b–d) show the coverage for the  $C_{20}OH$  and  $FC_{10}OH$  single surfactant systems with the transition temperature separated by the amount appropriate for systems B–D. Note that we have assumed that the domain coverage curves for these different concentrations will have the same shape as the curves measured by X-rays for the concentrations of  $15.0$  mmol/kg for  $C_{20}OH$  and  $5.0$  mmol/kg for  $FC_{10}OH$  shown in Figures 4 and 5. This assumption is not strictly correct, but it provides a basis for a simple prediction.

Panels e–h of Figure 16 provide a prediction for the behavior of domain coverage of  $C_{20}OH$  and  $FC_{10}OH$  in the mixed systems A–D. These predictions can be compared to panels i–l of Figure 16 that summarize the findings of Figures 12–15.

The predictions in panels e–h are based upon the change in entropy that occurs upon adsorption of either the  $C_{20}OH$  or  $FC_{10}OH$ . In the single surfactant systems the transition is an adsorption transition in which  $C_{20}OH$  or  $FC_{10}OH$  adsorbs to the interface as the temperature is lowered. The change in interfacial excess entropy across this transition  $\Delta S_a^\sigma$  is, therefore, a measure of the free energy change upon adsorption of  $C_{20}OH$  or  $FC_{10}OH$  molecules. The change  $\Delta S_a^\sigma$  is just the difference in values of  $S_a^\sigma$  on either side of the transition. For single surfactant  $C_{20}OH$ ,  $\Delta S_a^\sigma$  varies from  $1.93$  to  $2.13$  mJ/(m<sup>2</sup> K) (for concentrations of  $18.04$  to  $4.40$  mmol/kg, respectively) and for single surfactant  $FC_{10}OH$ ,  $\Delta S_a^\sigma$  varies from  $0.77$  to  $0.55$  mJ/(m<sup>2</sup> K) (for concentrations of  $7.02$ – $3.49$  mmol/kg, respectively). This indicates that adsorption of  $C_{20}OH$  is greatly favored over adsorption of  $FC_{10}OH$ .

The large difference in  $\Delta S_a^\sigma$  between  $C_{20}OH$  and  $FC_{10}OH$  provides a qualitative guide to superposing the single surfactant systems to predict the behavior of the mixed system. For example, at a temperature below the single surfactant  $C_{20}OH$  transition in system A (Figure 16a) both the  $C_{20}OH$  and  $FC_{10}OH$  single surfactant systems would have a coverage of nearly 1. Because the adsorption of  $C_{20}OH$  is greatly favored, in the mixed system it is expected that the interface is preferentially covered by  $C_{20}OH$ . Therefore, in our prediction for the mixed system (panels e–h) we sketch the low-temperature behavior as mimicking the single surfactant  $C_{20}OH$  behavior (as shown in panels a–d). This is consistent with our finding for systems A–C, that the lowest temperature phase has  $C_{20}OH$  coverage of nearly one (see panels i–k of Figure 9).

As the temperature for system A is increased above the  $C_{20}OH$  single surfactant system transition, the  $C_{20}OH$  coverage drops very rapidly to a coverage of 0. However, the coverage of the  $FC_{10}OH$  single surfactant system remains high for a temperature range of  $2$  °C above the  $C_{20}OH$  single surfactant system transition (between  $29$  and  $31$  °C). In that temperature range the interface can lower its free energy by adsorbing  $FC_{10}OH$  at a high coverage. This is similar to phase 2 of system A that has a coverage of  $FC_{10}OH$  of nearly one (panel i of Figure 16).

As the temperature of system A is raised further, our independent system approximation predicts the appearance of a transition from phase 2 to phase 3 in which the coverage of  $FC_{10}OH$  drops quickly from 1 to 0.6 and then drops slowly to 0.2. This is similar to our experimental results as seen by comparing panels e and i of Figure 16.

System D is similar to system A because the single surfactant transition temperature of  $FC_{10}OH$  is greater than that of  $C_{20}OH$  (Table 2). For system D these transition temperatures are separated by  $8$  °C (Table 2). Panels h and l indicate that we did not measure to low enough temperatures to observe the predicted phase 1 for system D.

For systems B and C the transition temperatures for the single surfactant  $C_{20}OH$  systems are slightly greater than that of the single surfactant  $FC_{10}OH$  system (Table 2). As seen in Figure 16, the persistence of a full monolayer of  $C_{20}OH$  to higher temperatures than the phase transition in single surfactant  $FC_{10}OH$  has the effect of removing phase 2 from the mixed surfactant system. The prediction for system C shown in panel g is qualitatively similar to the measured results shown in panel k. The primary failure of our simple prediction scheme occurs in phase 3 of system B. The results for system B in panel j indicate that more  $C_{20}OH$  than  $FC_{10}OH$  is present in phase 3, just the opposite of the prediction in panel g.

## Summary

We have studied the interface between water and mixed surfactant solutions of  $\text{CH}_3(\text{CH}_2)_{19}\text{OH}$  and  $\text{CF}_3(\text{CF}_2)_7(\text{CH}_2)_2\text{OH}$  in hexane. Three different values of the molal ratio of fluorinated to total surfactant concentration (0.25, 0.28, and 0.5) were studied over a range of total surfactant concentrations that varied from 0 to as large as 27 mmol/kg. Measurements of the interfacial tension as a function of temperature for these different compositions indicated the existence of three different phases. Values of the interfacial excess entropy of two of these phases agreed with values for the condensed monolayer phases at the interface between water and single surfactant solutions of either  $\text{CH}_3(\text{CH}_2)_{19}\text{OH}$  or  $\text{CF}_3(\text{CF}_2)_7(\text{CH}_2)_2\text{OH}$  in hexane.

X-ray reflectivity measurements from the liquid–liquid interface of these solutions confirms that two of the phases are condensed single surfactant monolayers of either  $\text{CH}_3(\text{CH}_2)_{19}\text{OH}$  or  $\text{CF}_3(\text{CF}_2)_7(\text{CH}_2)_2\text{OH}$  (phases 1 and 2, respectively). This identification was made both by direct comparison of the X-ray reflectivity from single surfactant and mixed surfactant systems and by determination of the electron density profile from the X-ray reflectivity. A simple layer model was used to determine the electron density profile. The layer thicknesses and electron densities agreed with values expected from the literature for the packing of fluorocarbon and hydrocarbon chains. The fluorocarbon chains of  $\text{CF}_3(\text{CF}_2)_7(\text{CH}_2)_2\text{OH}$  are close-packed in a solid monolayer phase whereas the hydrocarbon chains of  $\text{CH}_3(\text{CH}_2)_{19}\text{OH}$  have liquid ordering.

Identification of the phases with single surfactant monolayers was straightforward because the form of the X-ray reflectivity (and corresponding electron density profile) is very different for monolayers consisting of either  $\text{CH}_3(\text{CH}_2)_{19}\text{OH}$  or  $\text{CF}_3(\text{CF}_2)_7(\text{CH}_2)_2\text{OH}$ . This difference also facilitates the analysis of the interfacial structure when both kinds of surfactants are simultaneously present on the interface. However, analysis of X-ray reflectivity from the mixed surfactant interface is more challenging because, as we demonstrated, the two surfactants are not mixed homogeneously throughout the interfacial monolayer. To make progress with the analysis, we had to assume that  $\text{CH}_3(\text{CH}_2)_{19}\text{OH}$  and  $\text{CF}_3(\text{CF}_2)_7(\text{CH}_2)_2\text{OH}$  aggregate separately into single surfactant domains. We also assumed that the layer thicknesses and layer electron densities within each of the domains was the same as in a single surfactant monolayer. With these assumptions, all the data over a wide range of compositions could be analyzed using only fitting parameters that characterized the coverage of the  $\text{CH}_3(\text{CH}_2)_{19}\text{OH}$  and  $\text{CF}_3(\text{CF}_2)_7(\text{CH}_2)_2\text{OH}$  domains and the interfacial roughness.

This analysis determined that phase 3 contains  $\text{CH}_3(\text{CH}_2)_{19}\text{OH}$  and  $\text{CF}_3(\text{CF}_2)_7(\text{CH}_2)_2\text{OH}$  domains as well as gaseous regions of the interface with a very low density of surfactants. The fraction of  $\text{CH}_3(\text{CH}_2)_{19}\text{OH}$  domains is zero for three of the four compositions studied by X-ray reflectivity. The fourth composition (system B) contained a larger coverage of  $\text{CH}_3(\text{CH}_2)_{19}\text{OH}$  interfacial domains than  $\text{CF}_3(\text{CF}_2)_7(\text{CH}_2)_2\text{OH}$  domains even though the bulk fraction of  $\text{CF}_3(\text{CF}_2)_7(\text{CH}_2)_2\text{OH}$  was the same as for system A. This is an indication of the nonideal nature of these solutions, as noted by earlier studies.<sup>17</sup>

We also described a simple method for predicting qualitatively the coverage or interfacial density of the mixed surfactant system from the behavior of the single surfactant systems. This method is a valid approximation because the interface consists of domains that are primarily either  $\text{CH}_3(\text{CH}_2)_{19}\text{OH}$  and  $\text{CF}_3(\text{CF}_2)_7(\text{CH}_2)_2\text{OH}$ , with little mixing within a domain. The method relied upon a knowledge of the phase transition temperatures, the coverage or interfacial density, and the

measured change in interfacial excess entropy across the transitions for the single surfactant systems. Figure 16 illustrated the success of this approach which provides a simple understanding of the phase diagram of the mixed surfactant system.

**Acknowledgment.** We acknowledge conversations with Professor Dirk Morr (UIC Physics). This work was supported by the donors of the Petroleum Research Fund administered by the ACS, the UIC Campus Research Board, and the NSF Division of Materials Research. Brookhaven National Laboratory is supported by the U.S. Department of Energy.

## References and Notes

- (1) *Phenomena in Mixed Surfactant Systems*; Scamehorn, J. F., Ed.; American Chemical Society: Washington, DC, 1986.
- (2) *Mixed Surfactant Systems*; Holland, P. M., Rubingh, D. N., Eds.; American Chemical Society: Washington, DC, 1992.
- (3) *Mixed Surfactant Systems*; Ogino, K., Abe, M., Eds.; Marcel Dekker: New York, 1993.
- (4) Rosen, M. J. *Surfactants and Interfacial Phenomena*; Wiley: Hoboken, NJ, 2004.
- (5) Schlossman, M. L. *Curr. Opin. Colloid Interface Sci.* **2002**, *7*, 235.
- (6) Penfold, J.; Thomas, R. K.; Staples, E.; Tucker, I. In *Mesoscale Phenomena in Fluid Systems*; Case, F., Alexandridis, P., Eds.; ACS Symposium Series; American Chemical Society: Washington, DC, 2003; Vol. 861; p 96.
- (7) Richmond, G. L. *Chem. Rev.* **2002**, *12*, 2693.
- (8) Mukerjee, P.; Mysels, K. J. In *ACS Symposium Series 9*; American Chemical Society: Washington, DC, 1975; p 239.
- (9) Shinoda, K.; Nomura, T. *J. Phys. Chem.* **1980**, *84*, 365.
- (10) Kadi, M.; Hansson, P.; Almgren, M.; Bergstrom, M.; Garamus, V. M. *Langmuir* **2004**, *20*, 3933.
- (11) Kadi, M.; Hansson, P.; Almgren, M.; Furo, I. *Langmuir* **2002**, *18*, 9243.
- (12) Barthelemy, P.; Tomao, V.; Selb, J.; Chaudier, Y.; Pucci, B. *Langmuir* **2002**, *18*, 2557.
- (13) Amato, M. E.; Caponetti, E.; Martino, D. C.; Pedone, L. *J. Phys. Chem. B* **2003**, *107*, 10048.
- (14) Zhu, B. Y.; Zhang, P.; Wang, R. X.; Liu, Z. F.; Lai, L. H. *Colloids Surf. A* **1999**, *157*, 63.
- (15) Imae, T.; Takeshita, T.; Kato, M. *Langmuir* **2000**, *16*, 612.
- (16) Takiue, T.; Matsuo, T.; Ikeda, N.; Motomura, K.; Aratono, M. *J. Phys. Chem. B* **1998**, *102*, 4906.
- (17) Takiue, T.; Matsuo, T.; Ikeda, N.; Motomura, K.; Aratono, M. *J. Phys. Chem. B* **1998**, *102*, 5840.
- (18) Takiue, T.; Toyomasu, T.; Ikeda, N.; Aratono, M. *J. Phys. Chem. B* **1999**, *103*, 6547.
- (19) Takiue, T.; Toyomasu, T.; Ikeda, N.; Aratono, M. *J. Phys. Chem. B* **2000**, *104*, 7096.
- (20) Tikhonov, A. M.; Li, M.; Mitrinovic, D. M.; Schlossman, M. L. *J. Phys. Chem. B* **2001**, *105*, 8065.
- (21) Tikhonov, A. M.; Pingali, S. V.; Schlossman, M. L. *J. Chem. Phys.* **2004**, *120*, 11822.
- (22) Goebel, A.; Lunkenheimer, K. *Langmuir* **1997**, *13*, 369.
- (23) Mitrinovic, D. M.; Tikhonov, A. M.; Li, M.; Huang, Z.; Schlossman, M. L. *Phys. Rev. Lett.* **2000**, *85*, 582.
- (24) Matubayasi, N.; Motomura, K.; Kaneshina, S.; Nakamura, M.; Matuura, R. *Bul. Chem. Soc. Jpn.* **1977**, *50*, 523.
- (25) Eduljee, H. E.; Newitt, D. M.; Weale, K. E. *J. Chem. Soc.* **1951**, 3086.
- (26) Rine, R. A.; Millero, R. J. *J. Chem. Phys.* **1973**, *59*, 5529.
- (27) Zhang, Z.; Mitrinovic, D. M.; Williams, S. M.; Huang, Z.; Schlossman, M. L. *J. Chem. Phys.* **1999**, *110*, 7421.
- (28) Mitrinovic, D. M.; Williams, S. M.; Schlossman, M. L. *Phys. Rev. E* **2001**, *63*, 021601.
- (29) Schlossman, M. L.; Synal, D.; Guan, Y.; Meron, M.; Shea-McCarthy, G.; Huang, Z.; Acero, A.; Williams, S. M.; Rice, S. A.; Viccaro, P. J. *Rev. Sci. Instrum.* **1997**, *68*, 4372.
- (30) Pershan, P. S. *Faraday Discuss. Chem. Soc.* **1990**, *89*, 231.
- (31) Born, M.; Wolf, E. *Principles of Optics*, 6th ed.; Pergamon Press: Oxford, England, 1980.
- (32) Nevot, L.; Croce, P. *Rev. Phys. Appl.* **1980**, *15*, 761.
- (33) Buff, F. P.; Lovett, R. A.; Stillinger, F. H. *Phys. Rev. Lett.* **1965**, *15*, 621.
- (34) Gelfand, M. P.; Fisher, M. E. *Physica A* **1990**, *166*, 1.
- (35) Schlossman, M. L.; Tikhonov, A. M. In *Mesoscale Phenomena in Fluid Systems*; Case, F., Alexandridis, P., Eds.; Oxford University Press: New York, 2003; p 81.

- (36) Weeks, J. D. *J. Chem. Phys.* **1977**, *67*, 3106.
- (37) Abraham, F. F. *Phys. Rep.* **1979**, *53*, 93.
- (38) Sinha, S. K.; Sirota, E. B.; Garoff, S.; Stanley, H. B. *Phys. Rev. B* **1988**, *38*, 2297.
- (39) Braslau, A.; Pershan, P. S.; Swislow, G.; Ocko, B. M.; Als-Nielsen, J. *Phys. Rev. A* **1988**, *38*, 2457.
- (40) Braslau, A.; Deutsch, M.; Pershan, P. S.; Weiss, A. H.; Als-Nielsen, J.; Bohr, J. *Phys. Rev. Lett.* **1985**, *54*, 114.
- (41) Als-Nielsen, J.; McMorrow, D. *Elements of Modern X-ray Physics*; John Wiley & Sons: Hoboken, 2001.
- (42) Helm, C. A.; Tippmann-Krayer, P.; Mohwald, H.; Als-Nielsen, J.; Kjaer, K. *Biophys. J.* **1991**, *60*, 1457.
- (43) Schwickert, H.; Strobl, G.; Kimmig, M. *J. Chem. Phys.* **1991**, *95*, 2800.
- (44) Takiue, T.; Uemura, A.; Ikeda, N.; Motomura, K.; Aratono, M. *J. Phys. Chem.* **1998**, *102*, 3724.
- (45) Barton, S. W.; Goudot, A.; Bouloussa, O.; Rondelez, F.; Lin, B.; Novak, F.; Acero, A.; Rice, S. A. *J. Chem. Phys.* **1992**, *96*, 1343.
- (46) Li, M.; Tikhonov, A.; Schlossman, M. L. *Europhys. Lett.* **2002**, *58*, 80.
- (47) Marchenko, V. I. *JETP* **1986**, *63*, 1315.
- (48) Andelman, D.; Brochard, F.; Joanny, J.-F. *J. Chem. Phys.* **1987**, *86*, 3673.
- (49) McConnell, H. M. *Annu. Rev. Phys. Chem.* **1991**, *42*, 171.
- (50) Hildebrand, J. H.; Fisher, B. B.; Benes, H. A. *J. Am. Chem. Soc.* **1950**, *72*, 4348.
- (51) Goodman, J. W. *Statistical Optics*; John Wiley & Sons: New York, 1985.
- (52) Uredat, S.; Findenegg, G. H. *Langmuir* **1999**, *15*, 1108.
- (53) Defay, R.; Prigogine, I.; Bellemans, A.; Everett, D. H. *Surface Tension and Adsorption*; Longmans, Green & Co. Ltd.: London, 1966.
- (54) Tikhonov, A. M.; Schlossman, M. L. *J. Phys. Chem. B* **2003**, *107*, 3344.